Managing Trirhythmicity and Bifurcation in the fractional biological vibro-impact system under correlated noise

R. Mbakob Yonkeu, Norbert Marwan, R. Yamapi, Jürgen Kurths

Originally published as

Yonkeu, R.M., Marwan, N., Yamapi, R., Kurths, J. (2025): Managing Trirhythmicity and Bifurcation in the fractional biological vibro-impact system under correlated noise. - Nonlinear Dynamics, 113, 28155–28177.
https://doi.org/10.1007/s11071-025-11576-4

Managing Trirhythmicity and Bifurcation in the fractional biological vibro-impact system under correlated noise

R. Mbakob Yonkeu,[1,2,*] **Norbert Marwan**,[2] **R. Yamapi**,[3] and **Jurgen Kurths**[2,4]

[1] *Fundamental Physics Laboratory, University of Bamenda,*
Faculty of Science, Department of Physics,
PO Box 39, Bambili, NWR, Cameroon.
[2] *Potsdam Institute for Climate Impact Research (PIK),*
Member of the Leibniz Association, Telegraphenberg,
P.O. Box 601203, 14473 Potsdam,Germany
[3] *Fundamental Physics Laboratory, Department of Physics,*
Faculty of Science, University of Douala, Box 24 157 , Douala, Cameroon
[4] *Department of Physics, Humboldt University, 12 489 Berlin, Germany*

(Dated: October 24, 2025)

Abstract

Numerous studies have explored the complex behaviors of stochastic fractional-order multirhythmic models and stochastic vibro-impact multirhythmic models. However, discussions about stochastic trirhythmic systems that include both fractional derivative elements in acceleration and vibro-impact parameters are relatively rare. This paper focuses on managing the trirhythmicity and stochastic bifurcation of a new extended fractional biological vibro-impact system subjected to correlated noise. To start, we replace the viscoelastic force with damping and stiffness forces. This change allows us to eliminate the original trirhythmic system's discontinuity through a non-smooth transformation, resulting in a stochastic trirhythmic system with fractional derivatives. Subsequently we employ random averaging to obtain estimate analytical solutions. We discovered that characteristics like correlation time, restitution coefficient, and fractional derivative coefficient may contribute to stochastic bifurcation. Simply altering the fractional order or restriction variable causes the probability density function to move between unimodal, bimodal, and trimodal distributions, revealing the presence of stochastic bifurcations inside the fractional multirhythmic setup. Furthermore, our research highlights that controlling system parameters including fractional order, control parameter, restitution coefficient, and correlation time can effectively govern bifurcation behaviors. The strong alignment between the theoretical and numerical solutions obtained from the predictor-corrector algorithm, as well as between the theoretical solutions and Monte Carlo simulations, confirms the accuracy of our conclusions. Additionally, our findings suggest that the noise intensity level at which the maximum Lyapunov exponent changes sign is affected by the fractional order and restitution coefficient in the system parameters. We also demonstrate that as energy loss during impact increases, the likelihood of vibro-impact systems exhibiting chaotic behavior significantly rises.

Keywords: *trirhythmicity, correlated noise, vibro-impact system, fractional-order derivative*

PACS numbers:

PACS. 05.45.Df Fractals

PACS. 05.10.Gg Stochastic analysis methods (Fokker-Planck, Langevin, etc.)

PACS. 02.60.Cb Numerical simulation; solution of equations

PACS. 02.50.-r Probability theory, stochastic processes, and statistics.

*raoulmbakob@yahoo.com`Correspondingauthors`

I. INTRODUCTION

In a variety of nonlinear dynamical self sustained systems, multirhythmicity is a common and important feature [1–5]. Fractional derivatives are common in real-life situations and have been successfully applied in physics [5–9], mathematics [10], biology [11, 12], chemistry [13], economics [14], climate [15] and mechanics [4, 16] systems. It appears that fractional exponents grew from integer exponents. The fractional dynamics structure is a dynamic model governed by fractional-order derivatives, unlike everyday structures modeled through integer-order calculus [17, 18]. Regardless of the availability of fractional calculus equipment in many fields of science, fractional differential equations research remains a niche area of study due to the fact that fractional calculus, as an extension of classical calculus, can provide an effective tool to understand the inherent complexity of manifold nonlinear phenomena [4, 5, 11]. The above references display that fractional-order systems are regularly more appropriate than the classical integer-order models to explain the complex systems which have memory property etc. The dynamical behavior analysis of fractional-order systems has attracted growing interest from researchers [6–10].
As a typical non-smooth multirhythmic model, a vibro-impact model is involved in several fields, such as civil engineering [19] and machinery [20, 21], and has been closely related to daily life. Random elements will continually appear in practical engineering, and including random elements in this foundation will make its multirhythmic traits wealthy and complex [22–24]. Impact under dynamic loads is a dynamic phenomena produced through the repeatedly contact among the mechanical elements with clearance or kinematical constraint [25–27]. Impacts in various forms in nonlinear system have been used successfully for controlling high-amplitude vibration systems in many practical applications, such as in cutting tools, turbine blades and tall flexible structures like chimneys [27–29]. Impacts happen when the system's vibration amplitudes surpass critical thresholds. Researching vibro-impact issues in nonlinear dynamic systems is important for optimizing machinery with gaps, as well as for analyzing reliability and suppressing noise [30–33]. Numerous researchers have examined non-smooth elements in dynamic nonlinear systems [2, 34], leading to the emergence of the new field of study known as non-smooth system [19, 21, 25, 30]. As multirhythmic systems with impact dampers contain one or more impact pairs of components, they exhibit highly complex and diverse dynamic behavior due to their strong nonlinearity and

discontinuity. Over the last few years, vibro-impact issues have emerged as a fresh topic in nonlinear self sustained systems. Recent studies have focused on Hopf-bifurcations [35, 36], transient response [37, 38], stochastic responses [39–43], bifurcation analysis etc [41, 44–47]. The study of the stochastic response of vibro-impact systems has gained a lot of interest due to the unavoidable noise perturbation in practical phenomena, leading to the proposal of numerous effective methods. The VDP oscillator is widely studied in nonlinear dynamics and is a model for systems showing self-excited oscillations in physics [16], biology [12] and even economics [34]. This oscillator has seen a lot of improvement because it moved from monorhythmic to birhythmic model [3] and finally to trirhythmic model [12]. For stochastic non-smooth systems, with the help of a non-smooth variable transformation put forward by Zhuravlev [42], some researches [25, 30, 42, 43] developed the stochastic averaging approach to study the dynamic characteristics of vibro-impact systems excited by random perturbations. Recent developments in the VDP model have explored the dynamic vibro-impact analysis, incorporating different types of fractional derivatives and exposed to different types of noise. In their study, Yanwen et al employed a stochastic VDP vibro-impact system with fractional derivative damping and Gaussian white noise excitation to analyze the impact of noise excitation, restitution condition, and fractional derivative damping on response stationary probability density functions. Furthermore, YongGe et al analyzed a vibro-impact oscillator with two types of fractional derivative components [3], Li et al explored the stationary probability density functions of a Duffing-Van der Pol vibro-impact system driven by correlated Gaussian white noise [33], Li et al examined the stochastic behavior of a nonlinear vibro-impact system with viscoelastic term under wide-band noise [44], Xie et al studied the transient response of a nonlinear vibro-impact system under Gaussian white noise excitation [37], Kumar et al studied the bifurcation analysis of a vibro-impact Duffing-Van der Pol oscillator with rigid barriers [7] and Wang et al Examined the viscoelasticity of the vibro-impact system under fractional derivative [6].

It is emphasized that all the systems mentioned in previous references, which include the vibro-impact effect and fractional derivative, as well as in other studies, exhibit both monorhythmic and birhythmic patterns. To the authors' knowledge, there have been no studies on stochastic fractional trirhythmic biological vibro-impact systems with one kind of fractional derivative put on acceleration and subjected to Gaussian correlated noise. Inspiredly, we are motivated to study the bifurcation and trirhythmicity control in a fractional new modified trirhythmic vibro-impact system in the presence of correlated noise. The study centers on an in-depth investigation of the combined impact of fractional-order, correlation time, restitution coefficient, non-linear parameters, correlated noise intensity and control parameters on the trirhythmic zone, energy barriers in the trirhythmic system, Energy uptake, dissipipation, Hopf bifurcation, Lyapunov exponent and so on in the trirhythmic vibro-impact model. The rest of this work covers the following four sections: Section 2 discusses the system, presents a non-smooth transformation and the setup. In Section 3, the effect of system parameters on controlling trirhythmicity and energy barriers is studied. In section 4, the analysis of stationary probability density function, Hopf-bifurcation and Lyapunov exponent is presented and the conclusion of this work is given in Section 5.

II. SYSTEM DESCRIPTION, NON-SMOOTH TRANSFORMATION AND SETUP

A. Biological model and Equivalent vibro-impact system

Nonlinear systems can exhibit complex behavior, including chaos, bifurcation and so on [48, 49]. We handle a fractional self-sustaining trirhythmic biological vibro-impact system powered by correlated noise and a fractional derivative. The movements of the system is modulated by the following differential equation:

$$\begin{cases} \frac{d^{1+\lambda}U}{dt^{1+\lambda}} - \mu_0(1 - U^2 + \alpha_0 U^4 - \beta_0 U^6 + \gamma_0 U^8 - \delta_0 U^{10})\frac{dU}{dt} + \omega_0^2 U = \eta_0(t), \quad U > 0.0, \\ \dot{U}_+ = -r\dot{U}_-, \quad U = 0.0, \end{cases} \tag{1}$$

α_0, β_0, γ_0, and δ_0 represent positive indices which quantify the biological system's predisposition to ferroelectric instability. μ_0 is a positive factor whose role is to modulate the nonlinearity of the model. Besides, $\eta_0(t)$ is a additive correlated noise, with $< \eta_0(t) >= 0.0$ and $\{< \eta_0(t)\eta_0(t_0) >\} = \frac{D}{\tau}\exp\left(-\frac{|t-t_0|}{\tau}\right)$, where D and τ stand for the noise intensity and correlation time, respectively. The term $\frac{d^{\lambda+1}U}{dt^{\lambda+1}} = D^{\lambda+1}U$ denotes the fractional derivative in which λ is the fractional-order. It is worth noting that this is not merely a mathematical generalization, but the incorporation of fractional-oder derivation in eq.(1) is of modeling interest in the sense that it takes into account memory effects that are fundamental to almost every natural phenomenon. ω_0 is the typical frequency of the oscillator and r is the restitution coefficient. $\dot{U}_+$ and $\dot{U}_-$ denotes the velocities of the system after and before the impact, respectively. The value of r shows the degree of energy loss of the vibro-impact self sustained system, when collision occurs. In other words, the energy loss is extremely small when r approaches to 1.0, but significant as r nears 0.0. From the literature review, it appears that fractional vibro-impact van der Pol system can be used to model and analyze the behavior of impact dampers, which are used to control vibrations in mechanical systems, model and optimize vibration-based energy harvesting systems, which convert ambient vibrations into electrical energy or to model and analyze the dynamics of human gait, including the effects of nonlinearity and fractional order dynamics on gait stability and variability.

B. Expanding investigation of the fractional trirhythmical self-sustained model

Fractional calculus in mechanical systems extends integration and differentiation to a non-integer-order integro-differential operator ${}_pD_y^q$. What can be outlined as:

$$
{}_pD_y^q = \begin{cases} \frac{d^q}{dt^q} & if \;\; \Re(q) > 0.0, \\ 1.0 & if \;\; \Re(q) = 0.0, \\ \int_0^y (d\tau)^{-q} & if \;\; \Re(q) < 0.0, \end{cases} \tag{2}
$$

where the derivative order q can be a complex number, and $\Re(q)$ represents the real component of q. The numbers p and y represent the operator's bounds. Currently, there are various definitions for fractional derivatives, including the $Grunwald-Letnikov$, $Caputo$, $Riemann-Liouville$ and $Atangana-Baleanu$ formulations. In this investigation, we will employ $Caputo's$ concept, which describes fractional-order derivatives as follows:

$$
D^{\lambda}U(t) = \frac{1}{\Gamma(1-\lambda)}\int_0^t \frac{\dot{U}(\tau_1)}{(t-\tau_1)^{\lambda}}d\tau_1, \quad 0.0 < \lambda \leq 1.0, \tag{3}
$$

where $\Gamma(z) = \int_0^{+\infty} e^{-t}t^{z-1}dt$ denotes the Gamma function satisfying the following expression: $\Gamma(z+1) = z\Gamma(z)$. Additionally, the term $\frac{d^{\lambda}U(t)}{dt^{\lambda}} = D^{\lambda}U(t)$ accounts for the intrinsic damping vibration to the studied dynamics. It was shown in Refs.[3, 4, 11, 14] that the expression associated with fractional derivative can serve both as classical restoring and damping force. Hence, by appropriately implementing the harmonic function method, the expression for $D^{\lambda}U(t)$ can be substituted by the expression:

$$
D^{1+\lambda}U(t) = D\left(D^{\lambda}U(t)\right) = \omega_0^{\lambda-1}\sin\left(\frac{\lambda\pi}{2}\right)\ddot{U}(t) + \omega_0^{\lambda}\cos\left(\frac{\lambda\pi}{2}\right)\dot{U}(t), \tag{4}
$$

combining Eq.(4) with Eq.(1) yields the following comparable random expression:

$$
\begin{cases} \frac{d^2U}{dt^2} - \mu_1(\beta_1 - U^2 + \alpha_0U^4 - \beta_0U^6 + \gamma_0U^8 - \delta_0U^{10})\frac{dU}{dt} + \omega_1^2U = \beta_2\eta_0(t), \quad U > 0.0, \\ \dot{U}_+ = -r\dot{U}_-, \quad U = 0.0, \end{cases} \tag{5}
$$

where $\mu_1 = \frac{\mu_0\omega_0^{1-\lambda}}{\sin\left(\frac{\pi\lambda}{2}\right)}$, $\beta_1 = 1 - \frac{\omega_0^{\lambda}}{\mu_0}\cos\left(\frac{\pi\lambda}{2}\right)$, $\omega_1^2 = \frac{\omega_0^{3-\lambda}}{\sin\left(\frac{\pi\lambda}{2}\right)}$, $\beta_2 = \frac{\omega_0^{1-\lambda}}{\sin\left(\frac{\pi\lambda}{2}\right)}$

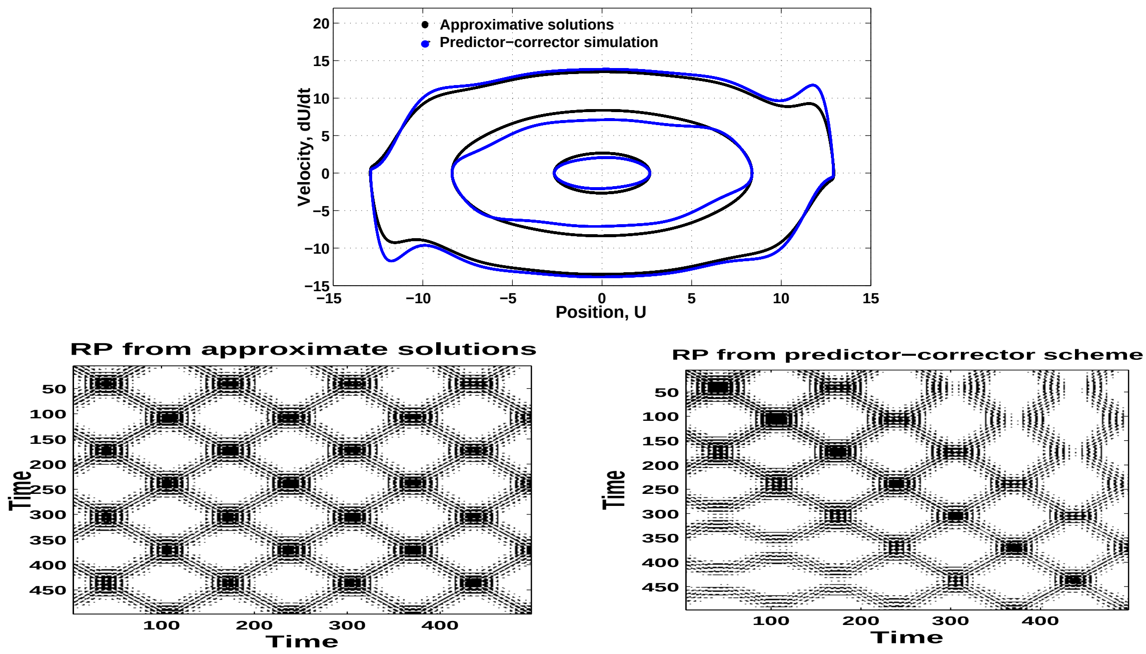

FIG. 1: Comparison of limit cycles plots and Recurrence plots between numerical solutions and approximate solutions with ordinary derivatives of fractional trirhythmic self-sustained system for a fixed value of the fractional-order parameter $\lambda = 0.997$ and when $(\alpha_0, \beta_0, \gamma_0, \delta_0) = (0.144, 0.005, 5.862.10^{-5}, 2.13.10^{-7})$, $r = 1.0$, $\omega_0 = 0.9$ and $\mu_0 = 0.002$.

C. Confirmation of the accuracy of analytical findings through the application of the predictor-corrector technique when $D = 0.0$ and $r = 1.0$

This subsection compares the computational results of Eqs. (1) and (5) when the noise intensity and the restriction coefficient are 0.0 and 1.0, respectively. Recurrence analysis of time series [50] is based on the examination of a matrix R whose members are defined as

$$R_{ij} = R_{ji} =^{1:\Phi_i \approx \Phi_j}_{0:\Phi_i \neq \Phi_j} \quad i, j = 1..N \tag{6}$$

where $\Phi(x, y)$ is the state vector, N is the length of the time series, and i and j are related to the line and column of the matrix, indicating equivalence up to an error ϵ. The elements of the matrix R are obtained by comparing the system's state at time i and j with a threshold precision of $\epsilon = 0.1$. The matrix is defined as follows:

$$R_{ij} = \theta(\epsilon - \|\Phi_i - \Phi_j\|), \tag{7}$$

with $\|(.)\|$ being the Euclidian norm and $\theta(\epsilon - \|\Phi_i - \Phi_j\|) = 1.0$ if $\epsilon > \|\Phi_i - \Phi_j\|$, $\theta(\epsilon - \|\Phi_i - \Phi_j\|) = 0.0$ if $\epsilon < \|\Phi_i - \Phi_j\|$ is the heaviside function.

In Fig.1, the phase portraits and recurrence plots are presented and we compare the numerical and approximative solutions for periodic oscillations when the fractional-order is 0.997. For the recurrence plots, we set the beginning scenario around the attractor's minimum amplitude. The approximative solution seems to align closely with the results of the numerical predictor-corrector simulations.

D. Non-smooth processing

The discontinuity in Eq.(1) can be eliminated by applying Zhuralev's mirror image transformation of state variables, which involves introducing non-smooth transformations of the state variables as follows:

$$U = U_1 = |Z| = Zsgn(Z), \quad \dot{U} = U_2 = \dot{Z}sgn(Z), \quad \ddot{U} = \ddot{Z}sgn(Z), \tag{8}$$

where $sgn(Z)$ is the signum function of Z, such that

$$sgn(Z) = \begin{cases} -1.0 & \text{for } Z < 0.0, \\ 0.0 & \text{for } Z = 0.0, \\ +1.0 & \text{for } Z > 0.0. \end{cases}$$

Obviously, the transformation Eq.(8) maps the domain $U > 0.0$ of the original phase plane $(U, \dot{U})$ onto the whole phase plane $(Z, \dot{Z})$, and makes the transformed velocity $\dot{Z}$ continuous when $r = 1.0$. Substituting some equations, the equations of the new variable can be written as follows:

$$\begin{cases} \frac{d^2Z}{dt^2} - \mu_1\left(\beta_1 - Z^2 + \alpha_0 Z^4 - \beta_0 Z^6 + \gamma_0 Z^8 - \delta_0 Z^{10}\right)\frac{dZ}{dt} + \omega_1^2 Z = \beta_2 sgn(Z)\eta_0(t), \quad t \neq t_*, \\ \dot{Z}_+ = r\dot{Z}_-, \quad t = t_*. \end{cases} \tag{9}$$

Here, the second relation of Eq.(9) is a constraint equation. Clearly, when $t = t_*$, there is a discontinuity in the velocity due to the impact when $r \neq 1.0$. The change in the velocity when $Z(t_*) = 0.0$ (at impact) is given by

$$(\dot{Z}_+ - \dot{Z}_-)\delta(t - t_*) = (1 - r)\dot{Z}|\dot{Z}|\delta(Z), \tag{10}$$

In this circumstance, one must regard the function $\delta(.)$ as a distribution function, which works on a significantly smooth function $\phi(t)$ to achieve $\int_{-\infty}^{\infty}\phi(s)\delta(s-t)ds = \phi(t^{-})$. In other words, The function $\delta(.)$ indicates that the velocity is estimated to be right before the effect of impact occurs. Take into account that the usual understanding of $\delta(.)$ as a Dirac-delta function requires that $\delta(.)$ can thus be used to deal with the vibro-impact constraint as an impulse damping of the governing model at each vibro-impact moment. This could lead to issues because there ought to be a discontinuous element $\dot{Z}|\dot{Z}|$ at $Z = 0$. The conversion in Equation (10) results in representing the impact's effect as a dissipation term described by the approximation

$$(1-r)\dot{Z}\delta(t-t_*) \approx (1-r)\dot{Z}|\dot{Z}|\delta(Z), \tag{11}$$

if $|\dot{Z}_+| < |\dot{Z}| < |\dot{Z}_-|$. Then the original impact oscillator of model (1) can be reduced to the following system without the impact term:

$$\frac{d^2Z}{dt^2} - \mu_1\left(\beta_1 - Z^2 + \alpha_0 Z^4 - \beta_0 Z^6 + \gamma_0 Z^8 - \delta Z^{10}\right)\frac{dZ}{dt} + (1-r)\dot{Z}|\dot{Z}|\delta(Z) + \omega_1^2 Z = \beta_2 sgn(Z)\eta_0(t) \tag{12}$$

E. Stochastic calculating technique

If $\mu_0, \alpha_0, \beta_0, \gamma_0, \delta_0$, $(1-r)$, and D are all tiny elements, then the solution of Eq. (12) has a periodic form. Consequently, for the slow varying amplitude $A_0(t)$ and phase $\theta_0(t)$, we establish the following expanded trial technique [5]:

$$\begin{aligned} Y_0 = Z(t) &= A_0(t)\cos\phi_0(t), \\ \dot{Y}_0 = v = \dot{Z}(t) &= -A_0(t)\omega_1 \sin\phi_0(t), \\ \phi_0(t) &= \omega_1 t + \theta_0(t), \end{aligned} \tag{13}$$

in which A_0, ϕ_0 and θ_0 being random processes. Taking the derivative of the above with respect to time results in

$$\dot{A}_0 \cos\phi_0 - A_0\dot{\theta}_0 \sin\phi_0 = 0. \tag{14}$$

Based on this, one can get the equations for the amplitude A_0 and the phase angle θ_0 from Eq.(12) as

$$\begin{aligned} \frac{dA_0}{dt} &= -\frac{1}{\omega_1}(f(Z,v) + sgn(Z)\beta_2\eta_0(t))sin\phi_0, \\ \frac{d\theta_0}{dt} &= -\frac{1}{A_0\omega_1}(f(Z,v) + sgn(Z)\beta_2\eta_0(t))cos\phi_0, \end{aligned} \tag{15}$$

where $f(Z,v) = \lambda_0 v$, with

$$\lambda_0 = \mu_1\Bigg(\beta_1 - Z^2 + \alpha_0 Z^4 - \beta_0 Z^6 + \gamma_0 Z^8 - \delta_0 Z^{10} - \frac{1}{\mu_1}(1-r)|\dot{Z}|\delta(Z)\Bigg). \tag{16}$$

centered on the random averaging concept [9], (A_0, θ_0) can be considered as a two-dimensional stochastic diffusion process. This allows for an estimation of the drift factor and the diffusion factor of the Fokker Planck formula through stochastic averaging and averaging over an oscillation period of $(2\pi/\omega_1)$:

$$\begin{aligned} \dot{A}_0 &= f(A_0) - \frac{\beta_1}{2\pi\omega_1}\int_0^{2\pi} \eta_0(t)\sin(\theta_0)d\theta_0, \\ \dot{\theta}_0 &= -\frac{\beta_1}{2\pi\omega_1 A}\int_0^{2\pi} \eta_0(t)\cos(\theta_0)d\theta_0, \end{aligned} \tag{17}$$

the expression $f(A_0)$ is defined in the following manner:

$$\begin{aligned} f(A_0) &= \frac{\mu_1 A_0}{1024}\Bigg[512\beta_1 - 128A_0^2 + 64\alpha_0 A_0^4 - 40\beta_0 A_0^6 + 28\gamma_0 A_0^8 - 21\delta_0 A_0^{10}\Bigg] \\ &- \frac{(1-r)\omega_1 A_0}{\pi}. \end{aligned} \tag{18}$$

If we consider $\Big[\mu_1(\beta_1 - Z^2 + \alpha_0 Z^4 - \beta_0 Z^6 + \gamma_0 Z^8 - \delta_0 Z^{10} + \frac{r-1}{\mu_1}|\dot{Z}|\delta(Z)|)\dot{Z}\Big]$ in Eq.(12) as an external force, in the context of energy, we obtain $E = \Big[\mu_1\Big(\beta_1 - Z^2 + \alpha_0 Z^4 - \beta_0 Z^6 + \gamma_0 Z^8 - \delta_0 Z^{10} + \frac{r-1}{\mu_1}|\dot{Z}|\delta(Z)|\Big)\dot{Z}^2\Big]$, over the period $0.0 \leq t \leq T (T \approx \frac{2\pi}{\omega_1})$, we write ΔE as

$$\begin{aligned} \Delta E &= E(T) - E(0) \\ &= \int_0^T \Bigg[\mu_1\Bigg(\beta_1 - Z^2 + \alpha_0 Z^4 - \beta_0 Z^6 + \gamma_0 Z^8 - \delta_0 Z^{10} + \frac{r-1}{\mu_1}|\dot{Z}|\delta(Z)|\Bigg)\dot{Z}^2\Bigg] dt. \end{aligned} \tag{19}$$

Using the foregoing analysis of Eq. (12), we get the following term:

$$\begin{aligned} \Delta E &= \pi A_0^2\Bigg[\frac{\mu_1 A_0}{1024}\Bigg[512\beta_1 - 128A_0^2 + 64\alpha_0 A_0^4 - 40\beta_0 A_0^6 + 28\gamma_0 A_0^8 - 21\delta_0 A_0^{10}\Bigg] \\ &- \frac{(1-r)\omega_1 A_0}{\pi}\Bigg]. \end{aligned} \tag{20}$$

The classic origin of correlated noise is a Gauss-Markov process characterized by exponential correlation is given as follows:

$$\begin{aligned} \dot{\eta_0} + \frac{1}{\tau}\eta_0 &= \frac{\sqrt(D)}{\tau} g_\omega, \\ < \eta(t)\eta(\phi_1) > &= S(t - \phi_1), \end{aligned} \tag{21}$$

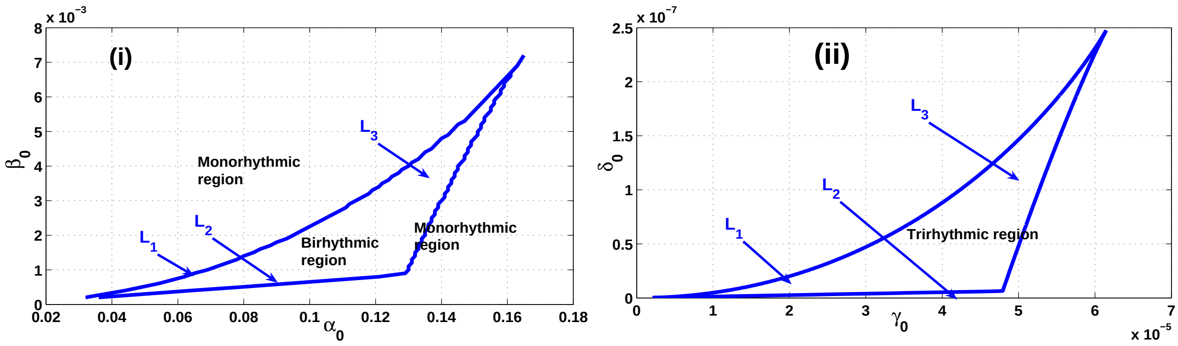

FIG. 2: Two variables bifurcation illustration of modified vdP oscillator in the variable plane $(\alpha_0,\ \beta_0)$ when $(\gamma_0,\ \delta_0) = (0.0,\ 0.0)$ (fig (i)) and $(\gamma_0,\ \delta_0)$ when $(\alpha_0,\ \beta_0) = (0.144,\ 0.005)$. The selected parameters are: $D = 0.0$,$r = 1.0$ $\mu_0 = 0.01$, $\omega_0 = 1.0$.

where $S(\rho) = S(-\rho) = \frac{2D}{1+\tau^2\rho^2}$ is believed to represent the power spectrum.

$$
\begin{aligned}
-\frac{1}{2\pi}\int_0^{2\pi} \eta_0(t)\sin(\theta_0)d\theta_0 &= \frac{1}{2\pi}\left[\eta_0(t)\cos(\theta_0)\right]_0^{2\pi} + \frac{1}{2\pi}\int_0^{2\pi} \dot{\eta_0}(t)\cos(\theta_0)d\theta_0, \\
&= \frac{\widetilde{D}}{2(1+\tau^2)} + \sqrt{\frac{D}{1+\tau^2}}\dot{W_{ie1}} \\
-\frac{1}{2\pi}\int_0^{2\pi} \eta_0(t)\cos(\theta_0)d\theta_0 &= \sqrt{\frac{D}{1+\tau^2}}\dot{W_{ie2}},
\end{aligned} \tag{22}
$$

$W_{ie1}(t)$ and $W_{ie2}(t)$ are separate normalized Wiener processes, and $\widetilde{D} = \frac{D}{A_0}$ denotes the dimensionless noise amplitude. The equations (17) clarify why attractors transition to escape states, based on the effective force $f(A_0)$, which is a gradient of an expression, implying the presence of a pseudo-potential. The expression for the effective pseudo-potential $U_{eff}(A_0)$ is as follows:

$$
\begin{aligned}
-U_{eff}(A_0) &= \frac{\mu_1}{1024}\left[256\beta_1 A_0^2 - 32A_0^4 + \frac{32}{3}\alpha_0 A_0^6 - 5\beta_0 A_0^8 + \frac{14}{5}\gamma_0 A_0^{10} - \frac{7}{4}\delta_0 A_0^{12}\right] \\
&\quad - \frac{(1-r)\omega_1 A_0^2}{2\pi} + \frac{\beta_2 D\ln(A_0)}{2\omega_1^2(1+\tau^2)}.
\end{aligned} \tag{23}
$$

Equation (23) demonstrates that the potential $U_{eff}(A_0)$ relies on the restitution coefficient r, the fractional-order λ, and the nonlinear parameter μ_0. Stationary oscillating entities are formed when $\partial U_{eff}/\partial A_0 = 0$. The corresponding amplitude equation fits the formula:

$$
\begin{aligned}
&- \beta_1 + \frac{1}{4}A_0^2 - \frac{\alpha_0}{8}A_0^4 + \frac{5}{64}\beta_0 A_0^6 - \frac{7}{128}\gamma_0 A_0^8 + \frac{21}{512}\delta_0 A_0^{10} + \frac{2(1-r)\omega_1}{\mu_1\pi} \\
&- \frac{\beta_2 D}{\mu_1(1+\tau^2)\omega_1^2 A_0^2} = 0.
\end{aligned} \tag{24}
$$

In Fig.2, we initial indicate in Fig.2(i) the area of (α_0, β_0) when $\gamma_0 = \delta_0 = 0.0$ of system (1) where the system admits three constructive solutions. Then, in Fig.2(ii), for (α_0, β_0) collected in the birhythmic area of Fig.2(i), we represent in parameter plane (γ_0, δ_0) the domain where system (1) in absence of noise has five constructive solutions. The saddle-node bifurcations correspond to L_1, L_2, and L_3 in Figs.2 (i) and (ii) that enclose the birhythmic and trirhythmic areas. The bifurcation line on the left (L_1) indicates the saddle-node bifurcation of the outer limit cycle, which is the high amplitude attractor, while the right line (L_3) signifies the saddle-node bifurcation of the inner limit cycle, which is the low amplitude attractor.

III. MANAGING TRIRHYTHMICITY AND ASSESSING ENERGY BARRIERS

A. Managing trirhythmicity by restriction coefficient and nonlinear term

The key characteristic of the nonlinear self-excited vibro-impact oscillator discussed in Eq.(1) is having multiple stable limit cycle solutions above two, displaying trirhythmicity depicted in Fig.2(ii) according to equation (25) in a noise-free scenario. By using the analytical estimate provided in equation (25), we can determine the number of positive roots that determine the existence of limit cycles. In Fig.3, the impact of the restitution factor in the trirhythmic zone of system (1), when (α_0, β_0) is taken in the birhythmic area of Fig.2(i), is presented. We find that a modest change of restitution coefficient r results in a significant shift in the trirhythmic zone. Alternatively, a decreasing value of r reduces the trirhythmic zone, and if this coefficient reaches a certain value, the system evolves into birhythmic. Fig.4 depicts the zones of dissipation $(f(A_0) > 0.0)$ and energy uptake $(f(A_0) < 0.0)$. It is clear that a limit cycle periodic response $f(A_0)$ should be zero, and the total number of solutions indicates either the existence or the absence of the number of limit cycles (periodic attractors) of this fractional vibro-impact system. Additionally, in this fractional multirhythmic system, the stability of the limit cycles can be tested by evaluating the derivative of the amplitude equation with respect to the amplitude and the stability implies $\left[\frac{df(A_0)}{dA_0}\right]_{Limit-cycle} < 0.0$. In the region of trirhythmicity, three stable periodic attractors A_{01}, A_{03} and A_{05} are present, and separated by the unstable attractors A_{02} and A_{04} as presented in Fig.4(a). It is clear that vibro-impact, as an external force on the fractional multirhythmic system, can effectively control the behavior of limit cycle oscillations. To study the effects of the restitution coefficient on the rhythmic properties of the oscillator, the plots of $f(A_0)$ versus amplitude for

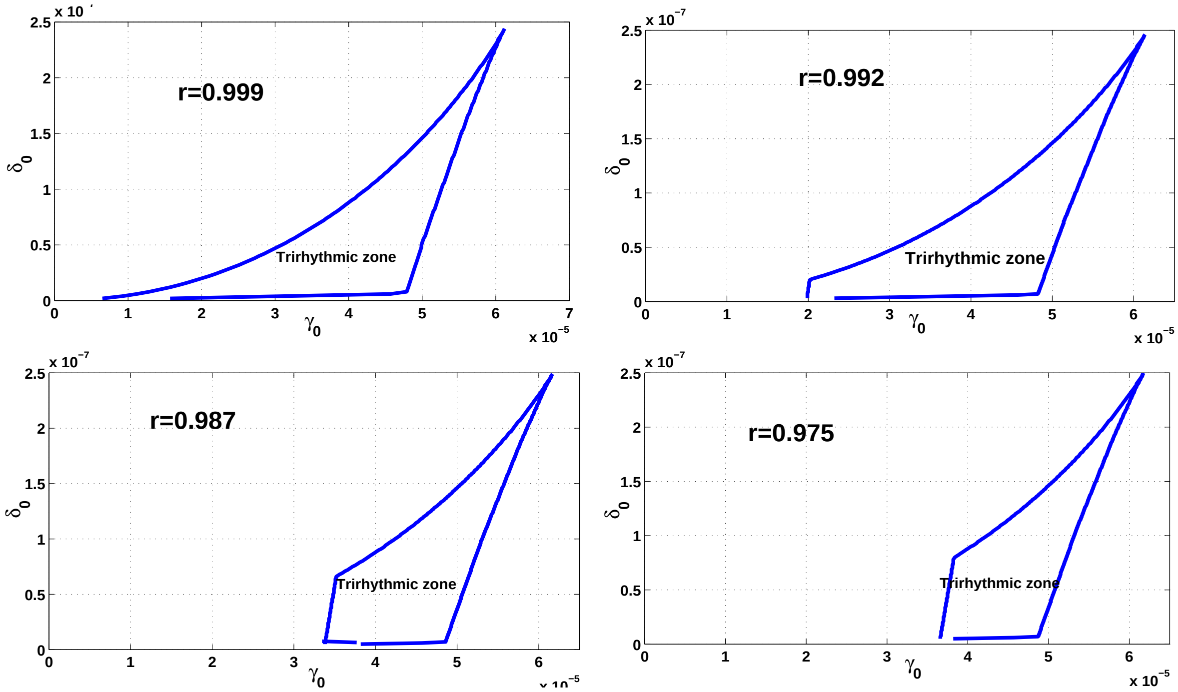

FIG. 3: Bifurcation determination of the trirhythmic vibro-impact system within (γ_0, δ_0) space showing the areas of birhythmicity and trirhythmicity for four values of vibro-impact coefficient when $(\alpha_0,\ \beta_0) = (0.144,\ 0.005)$. The specified parameters are: $D = 0.0$, $\mu_0 = 0.01$, $\lambda = 0.999$ $\omega_0 = 1.0$.

different values of r and for different control parameters $\alpha_0, \beta_0, \gamma_0, \delta_0$ are shown in Figs.4(b)-(d). Starting out, when the energy loss during the impact is extremely small, we detect five roots, indicating trirhythmicity in Fig.4. With a decrease in r to $r = 0.98$ (Fig.4(b)), the curve is gradually pushed downward and the roots are still five. As the value of r continues decreasing ($r = 0.96$), the curve is gradually pushed upward so that it crosses the zero line only once, exhibiting a three roots indicating two stable limit cycles or birhythmic behavior. As r further decreases, the curve is gradually pushed downward and the oscillation is recovered with the monorhythmic behavior and after a certain value of r ($r = 0.90$), the number of roots is zero, i.e. there are non-oscillations. This observation differs according to the control parameters $(\alpha_0, \beta_0, \gamma_0, \delta_0)$.

In Fig.5, we draw reliable bifurcation diagrams illustrating the amplitude A_0 dependency on r for various settings of the nonlinear parameter μ_0. Undoubtedly, the system has progressed from trirhythmic to birhythmic and, subsequently, to monorhythmic with decreasing r. The interval of r in which the system is trirhythmic depends strongly on the nonlinear parameter. In Fig.5(e), we observe that for $\mu_0 = 0.7$, the system is solely trirhythmic for all values of r and regardless the degree of energy lost after the impact.

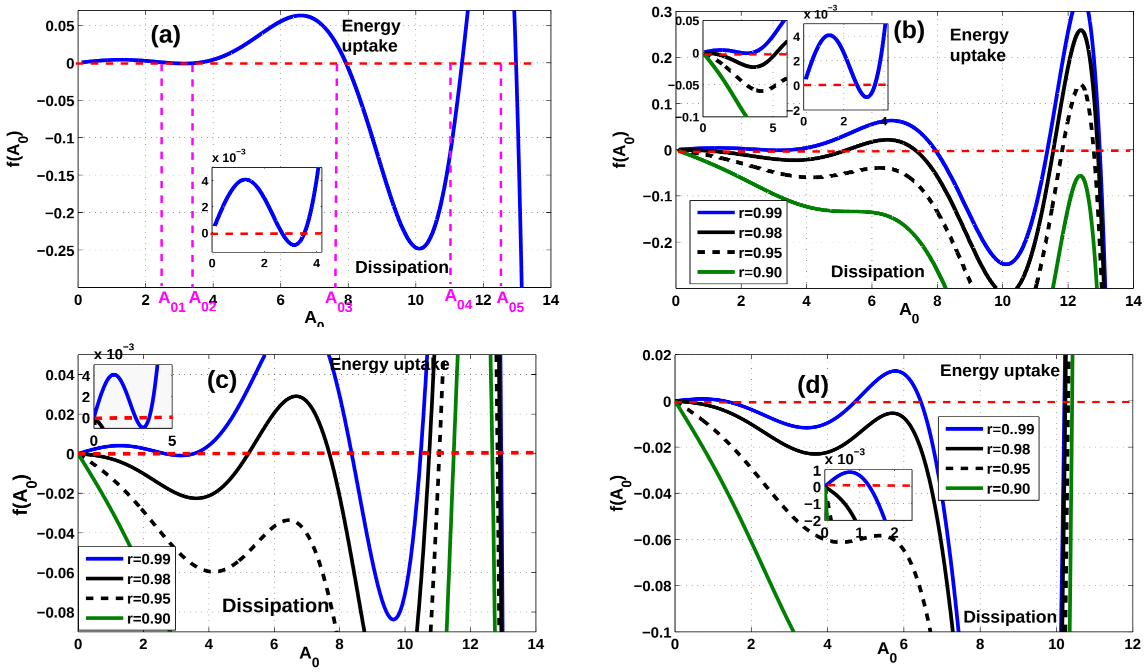

FIG. 4: Plot of amplitude equation f(A_0) versus amplitude A_0 .The areas of dissipation and energy uptake for different value of vibro-impact coefficient when $(\alpha_0,\,\beta_0,\,\gamma_0,\,\delta_0) = (0.144,\,0.005,\,5.7.10^{-5},\,2.10^{-7})$ (a, b), $(\alpha_0,\,\beta_0,\,\gamma_0,\,\delta_0) = (0.144,\,0.005,\,5.862.10^{-5},\,2.13.10^{-7})$(c) and $(\alpha_0,\,\beta_0,\,\gamma_0,\,\delta_0) = (0.144,\,0.005,\,4.3.10^{-5},\,1.10^{-7})$(d). The set parameters are $D = 0.0$, $\mu_0 = 0.01$, $\omega_0 = 1.0$, $\lambda = 0.998$.

B. Managing trirhythmicity by fractional-order derivative

Based on Eq.(25), Fig.6 shows the bifurcation graph in the (γ_0, δ_0) parameter plane by altering the fractional-order parameter λ at $r = 0.998$. This picture illustrates how λ affects the multi-rhythmic zone, exhibiting blue, green, and black patches representing monorhythmic, birhythmic, and trirhythmic regions, respectively. We found that all of these areas alter with a slight shift in λ. Specifically, the monorhythmic zone expands when λ drops, whereas the birhythmic and trirhythmic zones reduce.

C. Investigation of Energy Barriers throughout the Trirhythmic System

The benefit of using the quasi-potential in a multi-rhythmic system lies in its ability to encapsulate stability properties in a straightforward energy barrier, allowing for the extrapolation of

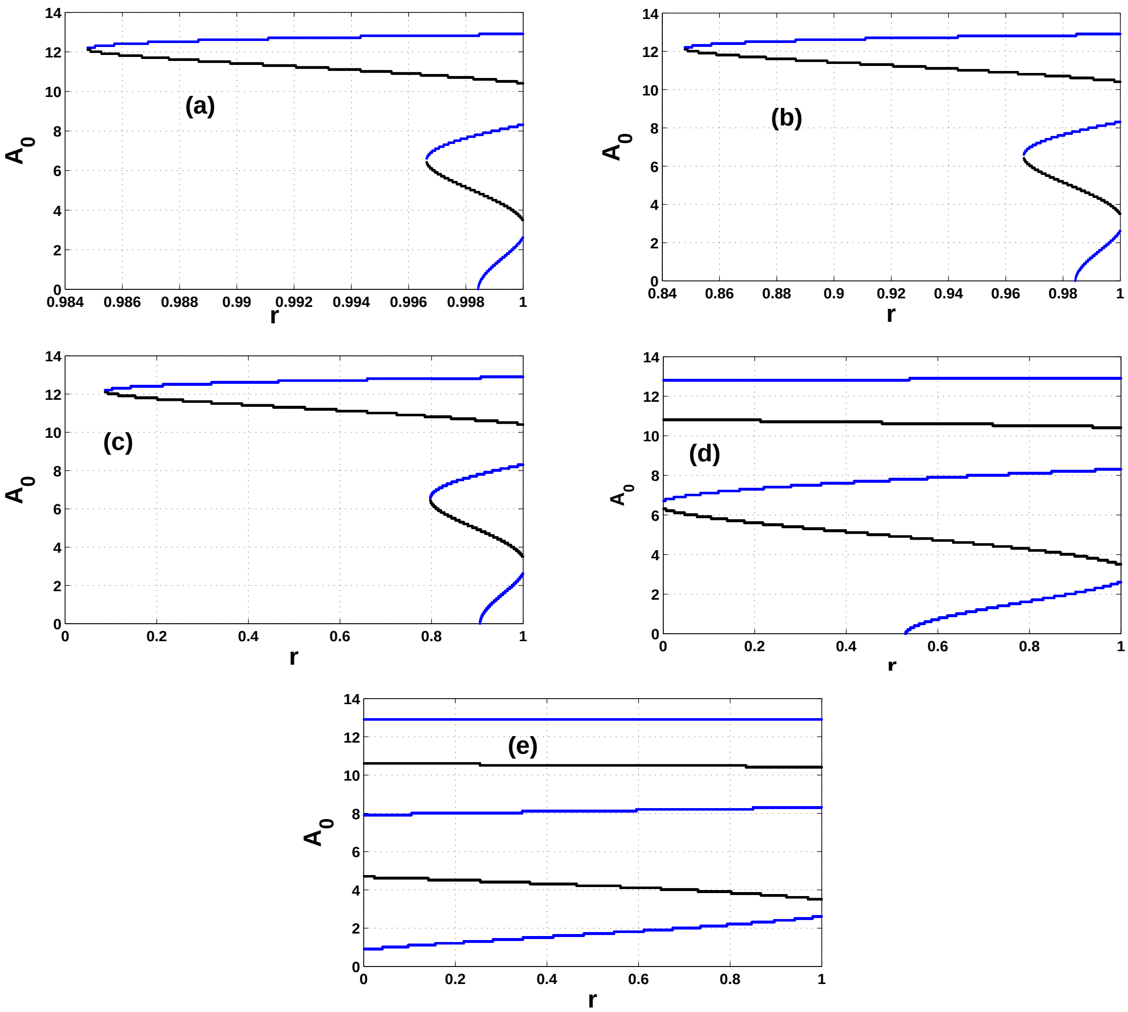

FIG. 5: nonlinear parameter impact on bifurcation diagram (with variation in r) when $\mu_0 = 0.001$ (a), $\mu_0 = 0.01$ (b), $\mu_0 = 0.04$ (c), $\mu_0 = 0.3$ (d), $\mu_0 = 0.7$ (e). The selected parameters are: $(\alpha_0,\ \beta_0,\ \gamma_0,\ \delta_0) = (0.144,\ 0.005,\ 5.862.10^{-5},\ 2.13.10^{-7})$, $D = 0.0$, $\omega_0 = 1.0$, $\lambda = 1.0$.

results from short escape times to rare events using Eq.(1), where correlated noise can provide the necessary energy to surpass a trapping potential. Hence, it is impossible to trap the system permanently within a well: Once fluctuations become large enough to surpass the barrier, the system exits the attractor's basin of attraction. Similarly, in oscillatory systems with three coexisting attractors, noise causes the attractors to become meta-stable and allows the system to randomly transition between them. When the three attractors are periodic cycles with varying durations, the system transforms into trirhythmic. The pseudo-potential is applicable in describing various physical characteristics of a specific system. When the fractional multirhythmic system is subjected to random fluctuations like correlated noise, in the case of five attractors (three stables and two unsta-

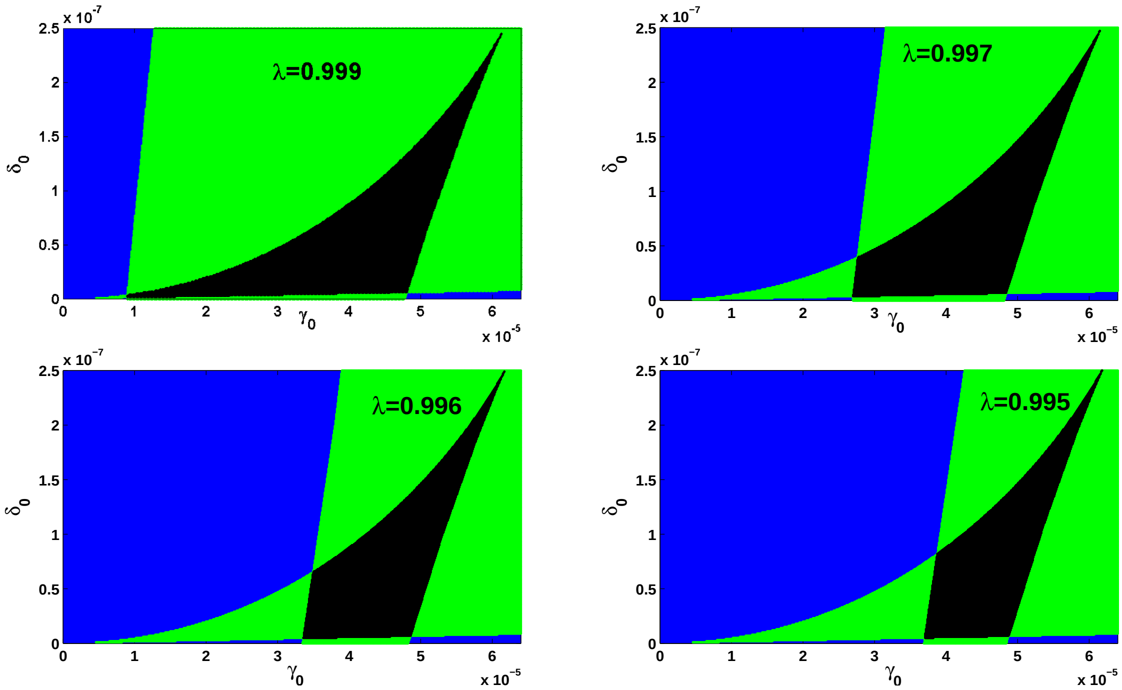

FIG. 6: The trirhythmic vibro-impact model's bifurcation in (γ_0, δ_0) space shows zones of monorhythmicity (blue), birhythmicity (green), and trirhythmicity (black) for four fractional-order parameter λ values when $(\alpha_0,\ \beta_0) = (0.144,\ 0.005)$. The selected parameters are $D = 0.0$, $\mu_0 = 0.01$, $r = 0.998$ $\omega_0 = 1.0$.

bles), a transition between the three stable attractors can happen, and a new kind of bifurcation is observed. In Fig.7, the effects of restitution coefficient and fractional-order on pseudo-potential of the fractional vibro-impact system are presented. According to eq.(23), the sketch of the effective pseudo-potential profile depending on λ and for self-sustained oscillator with multi-limit-cycles is given in Fig.7 for different value of r Fig.7(a) and λ Fig.7(b). We remark that when r decreases, the potential well in A_{01} tends to disappear and however, that one in A_{05} increases in depth rather and the quasi-same phenomena is observed with the variation of λ (see Fig.7(b)). It is also important to mention that the amplitudes A_{01}, A_{03} and A_{05} change very slightly when r or λ increases. Figure 8 depicts the energy barriers resulting from local stability via correlated noise-assisted hopping.

Indeed, correlated noise can provide sufficient energy to surpass a trapping potential ΔU_i, making it unfeasible to indefinitely confine the system in a well: Once fluctuations surpass the barrier, the system will exit the attractor's basin of attraction. Nevertheless, there are occasions when rhythmic processes may exhibit a more intricate behavior. One type of complicated oscillatory pattern is when three stable oscillatory patterns exist at the same time in the same external circumstances. Eq.(23) describes the behavior of effective energy barriers. We evaluated the energy

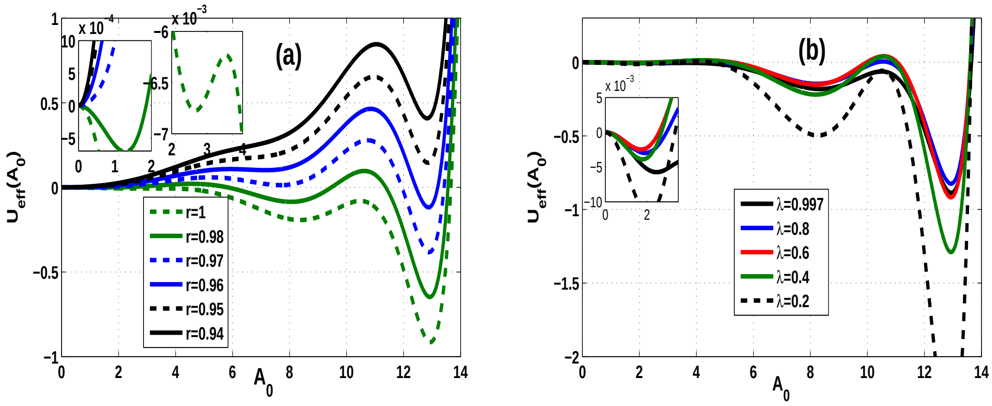

FIG. 7: Effect of restriction parameter (when $\lambda = 0.998$) and fractional-order (when $r = 0.998$) on the effective pseudo-potential. The selected parameters are $(\alpha_0, \beta_0, \gamma_0, \delta_0) = (0.144, 0.005, 5.862.10^{-5}, 2.13.10^{-7})$, $\mu_0 = 0.01$, $D = 0.0$.

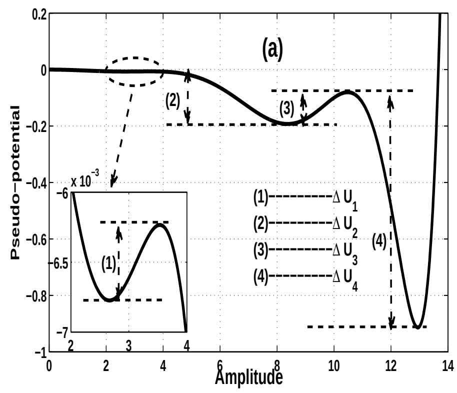

FIG. 8: Schematic illustration of the Energy barriers in an asymmetric meta-stable effective potential. ΔU_i are the corresponding activation energies. The selected parameters are $(\alpha_0, \beta_0, \gamma_0, \delta_0) = (0.144, 0.005, 5.862.10^{-5}, 2.13.10^{-7})$, $\mu_0 = 0.01$, $D = 0.24$, $\lambda = 0.999$, $r = 0.999$.

barriers using simulations in Fig.9, plotting the energy versus correlation time and fractional-order for two distinct restitution coefficient numbers. In this figure, ΔU_1, ΔU_2, ΔU_3 and ΔU_4 represent respectively the variation of energy that a particle needs to escape from the potential wells in A_{01}, A_{03}-to the left wells, A_{03}-to the right wells and A_{05}. It should be mentioned that according to the results found, excluding ΔU_3, the energy is lowered when r falls and for the increasing value of λ, ΔU_1, ΔU_3, ΔU_4 are increasing while ΔU_2 is decreasing. This is found for all values of correlation time taken between $[0, 5]$.

Our findings suggest that using effective trapping energy in a fractional vibro-impact system

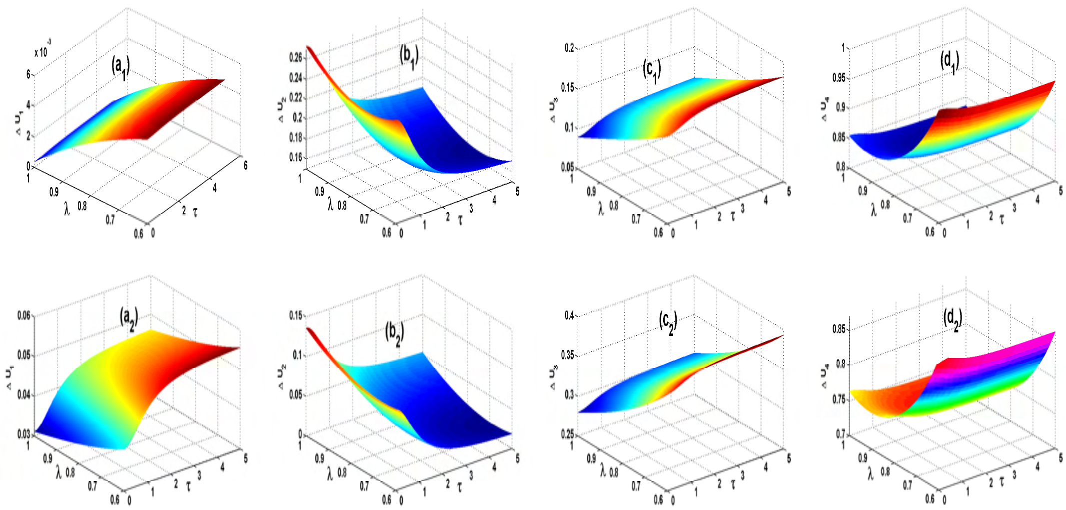

FIG. 9: *3D views of the resulting Energy barriers function ΔU_i of correlation time τ and fractional-order λ for two different values of restitution coefficient: (a_1), (b_1), (c_1), (d_1) and (a_2), (b_2), (c_2), (d_2) correspond respectively to $r = 0.998$ and $r = 0.990$. The others parameters are: $\mu_0 = 0.01$, $(\alpha_0, \beta_0, \gamma_0, \delta_0) = (0.144, 0.005, 5.82 \times 10^{-5}, 2.13 \times 10^{-7})$, $D = 0.25$.*

might enhance the global stability of trirhythmic attractors, even with correlated noise, vibro-impact value, and fractional derivatives.

IV. EXAMINATION OF STATIONARY PDFS, HOPF BIFURCATION AND LYAPUNOV EXPONENT

A. Stochastic Bifurcations in this fractional trirhythmic vibro-impact model

1. *Stochastic reactions*

In the limit of low noise intensity, $D << 1$, one can introduce the transformation equations Eqs.(13) to calculate the stationary Probability Distribution Function (PDF) of the amplitude of system (1). Moreover, the Fokker-Planck-Kolmogorov formula for the amplitude produces:

$$\frac{\partial P_r(A_0,t)}{\partial t} = -\frac{\partial}{\partial A}[m_1(A_0)P_r(A_0,t)] + \frac{1}{2}\frac{\partial^2}{\partial A_0^2}\left[\sigma_1(A_0)P_r(A_0,t)\right], \tag{25}$$

with

$$
\begin{aligned}
m_1(A_0) &= \frac{\mu_1 A_0}{1024}\left[512\beta_1 - 128A_0^2 + 64\alpha_0 A_0^4 - 40\beta_0 A_0^6 + 28\gamma_0 A_0^8 - 21\delta_0 A_0^{10}\right] \\
&\quad -\frac{(1-r)\omega_1 A_0}{\pi} + \frac{\beta_2 D}{2A_0\omega_1^2(1+\tau^2)}, \\
\sigma_1(A_0) &= \frac{\beta_2 D}{\omega_1^2(1+\tau^2)}.
\end{aligned}
\tag{26}
$$

Solving Eq.(25), the stationary PDF for the amplitude is given by the equation:

$$
\begin{aligned}
P_r(A_0) &= \frac{N_0}{\sigma_1(A_0)}\exp\left[\int_0^{A_0}\frac{2m_1(\varpi)}{\sigma_1(\varpi)}d\varpi\right] \\
&= \frac{N\omega_1^2 A_0(1+\tau^2)}{\beta_2 D}\exp\left[\frac{\mu_1\omega_1^2(1+\tau^2)}{512\beta_2 D}\left(256\beta_1 A^2 - 32A_0^4 + \frac{32\alpha_0}{3}A_0^6 - 5\beta_0 A_0^8 + \frac{14\gamma_0}{5}A_0^{10}\right.\right. \\
&\quad \left.\left. -\frac{7\delta_0}{4}A_0^{12}\right) - \frac{(1-r)\omega_1^3 A_0^2}{\pi\beta_2 D}\right],
\end{aligned}
\tag{27}
$$

where N_0 is the normalization unvarying, adheres to:

$$
\begin{aligned}
N_0 &= \left[\int_0^\infty \frac{\omega_1^2 A_0(1+\tau^2)}{\beta_2 D}\exp\left[\frac{\mu_1\omega_1^2(1+\tau^2)}{512\beta_2 D}\left(256\beta_1 A_0^2 - 32A_0^4 + \frac{32\alpha_0}{3}A_0^6 - 5\beta_0 A_0^8 + \frac{14\gamma_0}{5}A_0^{10}\right.\right.\right. \\
&\quad \left.\left.\left. -\frac{7\delta_0}{4}A_0^{12}\right) - \frac{(1-r)\omega_1^3 A_0^2}{\pi\beta_2 D}\right]dA_0\right]^{-1}.
\end{aligned}
\tag{28}
$$

Then the stationary PDF of the total energy is given as follows $H = Q(A_0) = \frac{1}{2}\omega_1^2 A_0^2$ can be retrieved so that

$$
P_r(H) = P_r(A_0)\left|\frac{dA_0}{dH}\right| = \frac{P_r(A_0)}{\omega_1^2 A_0}\Bigg|_{A_0 = Q^{-1}(H)}, \tag{29}
$$

The fundamental estimation for the joint probability density of displacement and velocity can be obtained as follows:

$$
\begin{aligned}
P_{rY_0,\dot{Y}_0}(Z,\dot{Z}) &= \frac{P_r(H)}{T_r(H)}\Bigg|_{H=\frac{1}{2}\omega_1^2 Z^2 + \frac{1}{2}\dot{Z}^2} \\
&= \frac{N_0\omega_1(1+\tau^2)}{2\pi\beta_2 D}\exp\left[\frac{\mu_1\omega_1^2(1+\tau^2)}{512\beta_2 D}\left\{256\beta_1\left(Z^2+\frac{\dot{Z}^2}{\omega_1^2}\right) - 32\left(Z^2+\frac{\dot{Z}^2}{\omega_1^2}\right)^2\right.\right. \\
&\quad + \frac{32}{3}\alpha_0\left(Z^2+\frac{\dot{Z}^2}{\omega_1^2}\right)^3 - 5\beta_0\left(Z^2+\frac{\dot{Z}^2}{\omega_1^2}\right)^4 + \frac{14}{5}\gamma_0\left(Z^2+\frac{\dot{Z}^2}{\omega_1^2}\right)^5 \\
&\quad \left.\left. -\frac{7}{4}\delta_0\left(Z^2+\frac{\dot{Z}^2}{\omega_1^2}\right)^6\right\} - \frac{(1-r)\omega_1^3(1+\tau^2}{\pi\beta_2 D}\left(Z^2+\frac{\dot{Z}^2}{\omega_1^2}\right)\right],
\end{aligned}
\tag{30}
$$

in which $T_r(H) = \frac{2\pi}{\omega_1}$. The joint stationary PDF of the original displacement U_1 and velocity U_2 ought to be calculated by doing the following:

$$P_r(U_1, U_2) = 2P_{rY_0,\dot{Y}_0}(U_1, U_2), \text{ and } U_1 \geq 0. \tag{31}$$

The stationary PDFs of displacement U_1 and velocity U_2 can be used to detect stochastic P_r-bifurcation by analyzing the variations in the number of extreme points in the PDF. Based to the singularity hypothesis [9, 12], the modification of the extreme value of the PDF must satisfy two conditions:

$$\frac{\partial P_r(A_0)}{\partial A_0} = 0, \text{ and } \frac{\partial^2 P_r(A_0)}{\partial A_0^2} = 0. \tag{32}$$

To achieve this goal, we may revise the PDF of amplitude as

$$P_r(A_0) = N_0 L_0(A_0, \alpha_0, \beta_0, \gamma_0, \delta_0, r, \mu_0, D, \tau, \lambda) \times \exp(S(A_0, \alpha_0, \beta_0, \gamma_0, \delta_0, r, \mu_0, D, \tau, \lambda)), \tag{33}$$

in which

$$\begin{aligned} L_0(A_0, \alpha_0, \beta_0, \gamma_0, \delta_0, r, \mu_0, D, \tau, \lambda) &= \frac{\omega_1^2 A_0(1+\tau^2)}{\beta_2 D}, \\ S(A_0, \alpha_0, \beta_0, \gamma_0, \delta_0, r, \mu_0, D) &= \frac{\omega_1^2(1+\tau^2)}{\beta_2 D}\left[\frac{\mu_1}{512}\left(256\beta_1 A_0^2 - 32A_0^4 + \frac{32\alpha_0}{3}A_0^6 - 5\beta_0 A_0^8\right.\right. \\ &\quad \left.\left. + \frac{14\gamma_0}{5}A_0^{10} - \frac{7\delta_0}{4}A_0^{12}\right) - \frac{(1-r)\omega_1 A_0^2}{\pi}\right]. \end{aligned} \tag{34}$$

The Both relations Eqs. (32) and (34 provide the following two constraints:

$$M_0 = \{L_0' + L_0 S' = 0.0, L_0'' + 2L_0' S' + L_0 S'' + L_0 S'^2 = 0.0\}, \tag{35}$$

where M_0 represents the state of change in the peak heights of the PDF shape. By substituting equations (34) with equations (35), we can determine the necessary parameters for a random P-bifurcation, including λ, r, μ, and the correlated noise parameters D and τ.

$$\begin{aligned} D &= \frac{\omega_1^2(1+\tau^2)}{\beta_2}\left[\mu_1\left(-\beta_1 A_0^2 + \frac{1}{4}A_0^4 - \frac{1}{8}\alpha_0 A_0^6 + \frac{5}{64}\beta_0 A_0^8 - \frac{7}{128}\gamma_0 A_0^{10} + \frac{21}{512}\delta_0 A_0^{12}\right)\right. \\ &\quad \left. + \frac{2(1-r)\omega_1 A_0^2}{\pi}\right], \end{aligned} \tag{36}$$

where the amplitude A_0 guarantees:

$$\mu_1(-128\beta_1 A_0^2 + 96\alpha_0 A_0^4 - 80\beta_0 A_0^6 + 70\gamma_0 A_0^8 - 63\delta_0 A_0^{10}) + 256\left(\mu_1 - \frac{2(1-r)\omega_1}{\pi}\right) = 0.0 \tag{37}$$

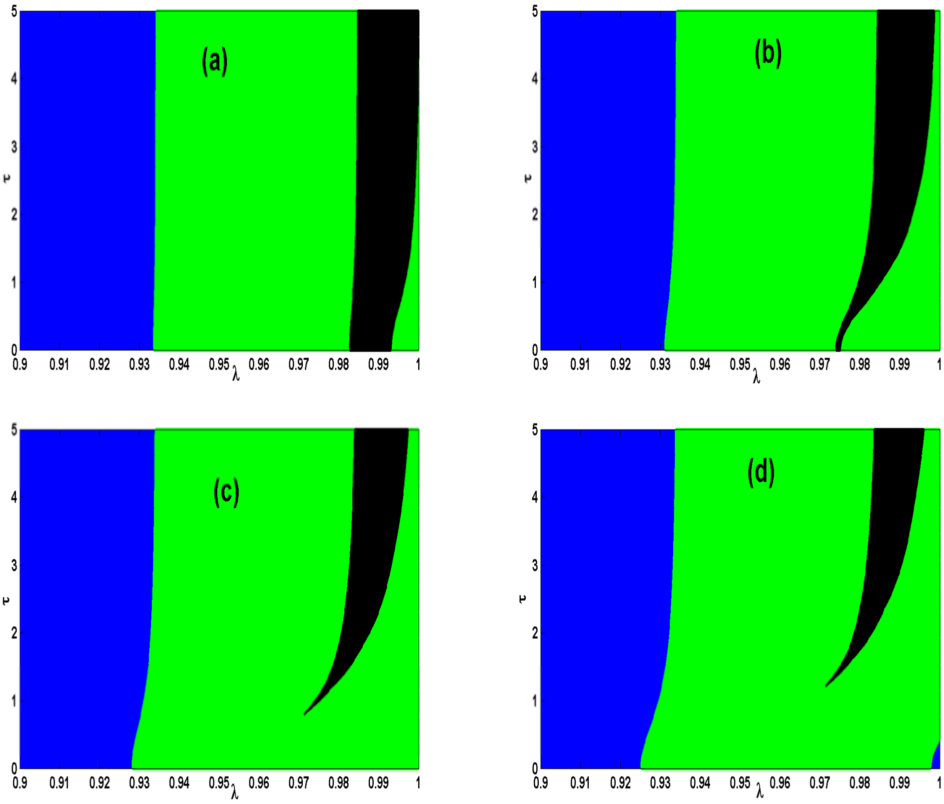

FIG. 10: Bifurcation diagram in parameter plane (λ, τ) for four different values of correlated noise intensity: (a), (b), (c) and (d) correspond respectively to $D = 0.05$, $D = 0.3$, $D = 0.7$, $D = 1.2$. The selected parameters are $(\alpha_0, \beta_0, \gamma_0, \delta_0) = (0.144, 0.005, 5.862.10^{-5}, 2.13.10^{-7})$, $\mu_0 = 0.01$, $\omega_0 = 0.9$.

2. Regulating bifurcation with fractional order derivatives and correlated noise

In this subsection, the fractional-order is used as the bifurcation parameter to investigate the impact of colored noise on the random response in the fractional-order trirhythmic vibro-impact system. Moreover, the impact of fractional-order term on vibration properties of the fractional vibro-impact system is demonstrated. In the variable plane of τ and λ, Fig.10 depicts the bifurcation schematic from the study of equations (36) and (37). In this figure, the effect of the correlated noise intensity on the domain (λ, τ), where the fractional vibro-impact system present a multirhythmic behavior, is shown. The stationary amplitude pattern is trimodal in the black area, bimodal in the green area, and unimodal in the blue area. The trirhythmic region in the parameters (λ, τ)-plane decreases with increasing correlated noise

Figure 11 compares the predictor-corrector algorithm to the analytical answer Fig.11(a) and

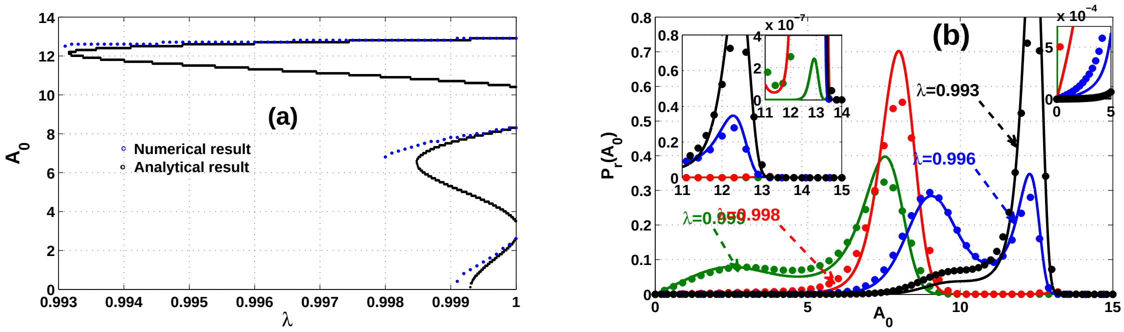

FIG. 11: (a): Analytical and predictor corrector simulation of Amplitude versus fractional-order. (b): Analytical and $MonteCarlo$ investigation of stationary density function for different values of λ. The selected parameters are: $(\alpha_0, \beta_0, \gamma_0, \delta_0) = (0.144, 0.005, 5.862.10^{-5}, 2.13.10^{-7})$ $D = 0.1$, $\tau = 0.5$.

Monte-Carlo predictions to the analytical approach Fig.11(b). In Fig.11(a), we display the fluctuation of the amplitude of the limit cycles in function of fractional-order employing the predictor-corrector approach (dotted lines) and analytical solution (solid line), and we discover that the number of limit cycles alters with the shift of λ. Figure 11(b) shows the change of the PDF vs amplitude for four different values of λ employing numerical Monte Carlo calculations (dotted line) and analytical calculation (solid line). The PDF of the previous fractional vibro-impact system (1) for amplitude may have one, two, or three peak levels, demonstrating the shift between one peak and three peaks with modifying λ, contributing to a stochastic P-bifurcation.

3. *Regulating bifurcation using restitution parameter*

From equations (36) and (37) we find for established values of $(\alpha_0, \beta_0, \gamma_0, \delta_0)$ taken in the tristable surface the areas of the parameter plane (r, μ_0), (λ, r), where the fractional vibro-impact system is trirhythmic or birhythmic. To estimate the implications of such correlated noise, r, λ, from formulas (36) and (37), for selected values of $(\alpha_0, \beta_0, \gamma_0 \delta_0)$ collected in the tristable surface, we present in Fig.12 the bifurcation graphic for a given parameter plane (μ_0, r) (Fig.12(a) and (b)) and (λ, r) (Fig.12(c) and (d)) and the study examines how μ_0, ω_0, r, and λ affect trirhythmic, birhyhmic, and monorhythmic action. Specifically, as anticipated by the evaluation of Eq.(25), we determine that decreasing ω_0 decreases the trirhythmic section in the variable plane (μ_0, r) and increases the trirhythmic portion in the parameter plane (λ, r). regardless of whether the values of the parameters $(\alpha_0, \beta_0, \gamma_0, \delta_0)$ are picked within the trirhythmic range, modifying various variables

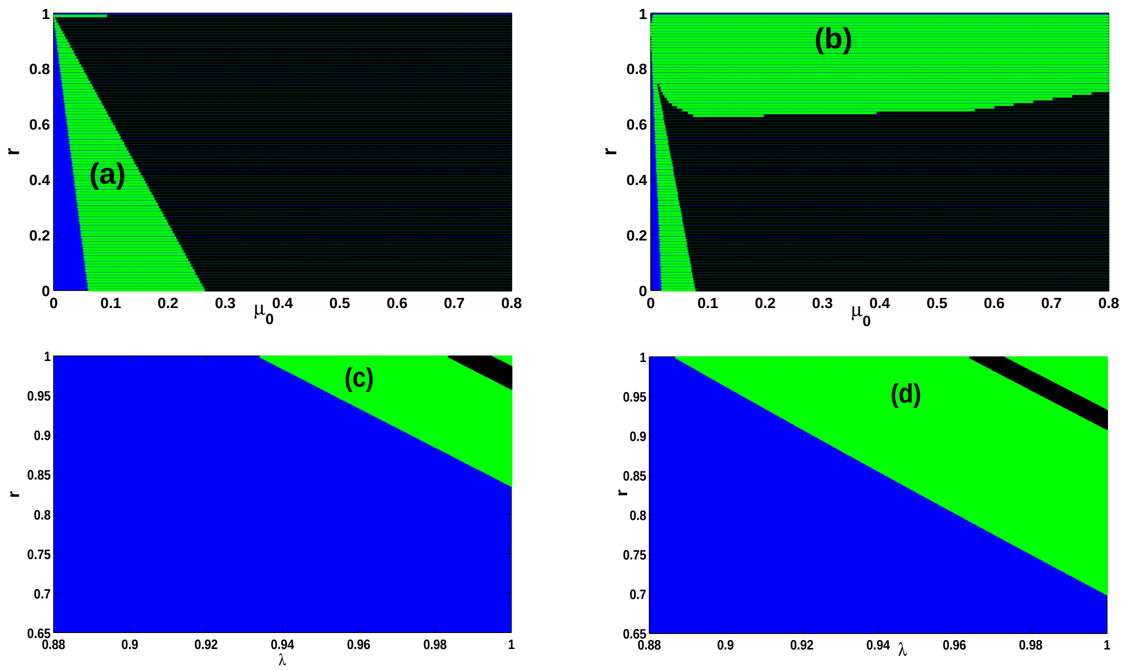

FIG. 12: Bifurcation investigation of the trirhythmic vibro-impact model in parameter plane (μ_0, r) (figures a and b) for $\lambda = 0.995$ and in parameter plane (λ, r) (figures c and d) when $\mu_0 = 0.01$ depicting the areas of monorhythmicity (blue surface), birhythmicity (green surface) and trirhythmicity (black surface) for two values of natural frequency ω_0 ($\omega_0 = 0.9$ (figures a and c) and $\omega_0 = 0.9$ (figures b and d)) when $(\alpha_0, \beta_0, \gamma_0, \delta_0) = (0.144, 0.005, 5.862.10^{-5}, 2.13.10^{-7})$. The selected parameters are $D = 0.1$, $\tau = 0.5$.

such as λ, r, μ_0, etc. leads the model to revert back to the monorhythmic situation. In overall, singularity hypothesis suggests that the topological designs of stationary probability trajectories at different places (r, λ) change with modest modifications in frequency and nonlinear component.

Considering the restitution coefficient serving as a bifurcation parameter, this part concentrates on the regulation of stochastic bifurcations by r using theoretical answers (33) and (34). Furthermore, the $predictor - corrector$ algorithm performs Monte Carlo numerical simulations of the fundamental fractional-order multirhythmic model (1), resulting in the stationary PDF. As demonstrated in Fig.13, the stationary PDF was applied to address the bifurcation regulation using multiple restitution coefficients and two different nonlinear parameters. $P_r(A)$ exhibits three peaks at $r = 0.99$ and $\mu_0 = 0.005$. With a subsequent decrease of r, for example when $r = 0.97$ or 0.96, we notice two peaks that have distinct behavior, and when $r = 0.84$, both other peaks disappear, leaving only one peak. On the other hand, when $\mu_0 = 0.2$, we change r between 0.7 and 0.999 and we note that the three peaks endure but have a different behavior and the shift between trimodal

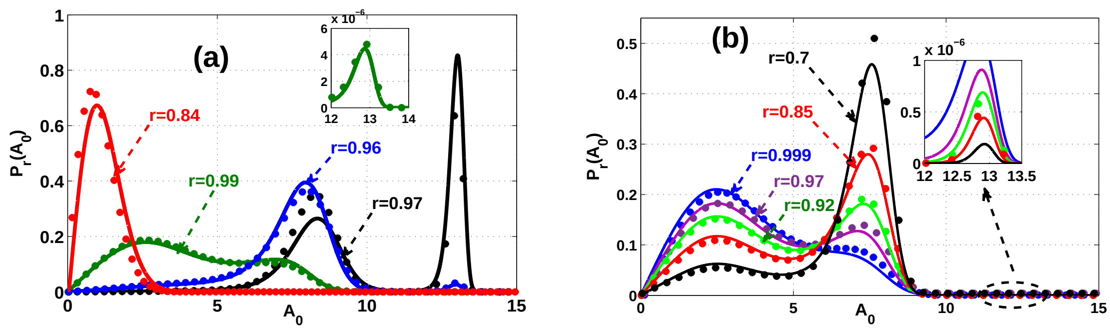

FIG. 13: Analytical and $MonteCarlo$ investigation of stationary density function for different values of restitution coefficient and for two different values of nonlinear parameter ((a) corresponds to $\mu_0 = 0.005$ and (b) corresponds to $\mu_0 = 0.2$). The selected parameters are: $(\alpha_0, \beta_0, \gamma_0, \delta_0) = (0.144, 0.005, 5.862.10^{-5}, 2.13.10^{-7})$ $D = 0.1$, $\tau = 0.5$.

to unimodal distribution is not observed in this case. Choosing a point (r, μ_0) or (r, λ) in each region results in a complete set of different stationary PDF graphs. The existence of r can shift the stationary probability density function from a unimodal to a trimodal distribution, indicating a stochastic P-bifurcation. This regulates the onset of bifurcation mechanisms. The consistency between analytical approaches and Monte Carlo simulation findings validates the theoretical analysis in this newly developed system. Figure 14 shows how r affects the joint PDF of U displacement and Z velocity. A near-doubling of r causes significant changes in the joint PDF, with a gradual shift in λ resulting in an enhancement from a vast crater (with $r = 0.92$) to four separate peaks (with $r = 0.999$). In the biological scenario, projecting joint PDFs reveals that a greater restitution coefficient causes the distribution to move to a lower Z value for a given number of enzyme molecules U. As a result, the rate of the chemical process slows down. Furthermore, when comparing the graphs 13 and 14, it is readily apparent that in this fractional vibro-impact setup, the joint probability density functions reveal an extremely intricate pattern, with the trimodal form of amplitude distribution probably corresponding to the respective three-peak or four-peak joint PDF.

The parametric surface where the PDF exhibits trimodality is enclosed by an approximately triangular area, as depicted in Fig.12. Taking the parameter in consideration: i) the PDFs for $P_r(A_0)$ and $P_r(U, Z)$ exhibit a stable limit cycle in the blue area, as depicted in Figs. 13 and 14, with the system's steady-state response characterized mainly by high-amplitude vibrations; ii) in the black region, the PDFs for $P_r(A_0)$ and $P_r(U, Z)$ display three stable limit cycles, reflecting equilibrium in the fractional system, thereby indicating three more probable motions in the system's response,

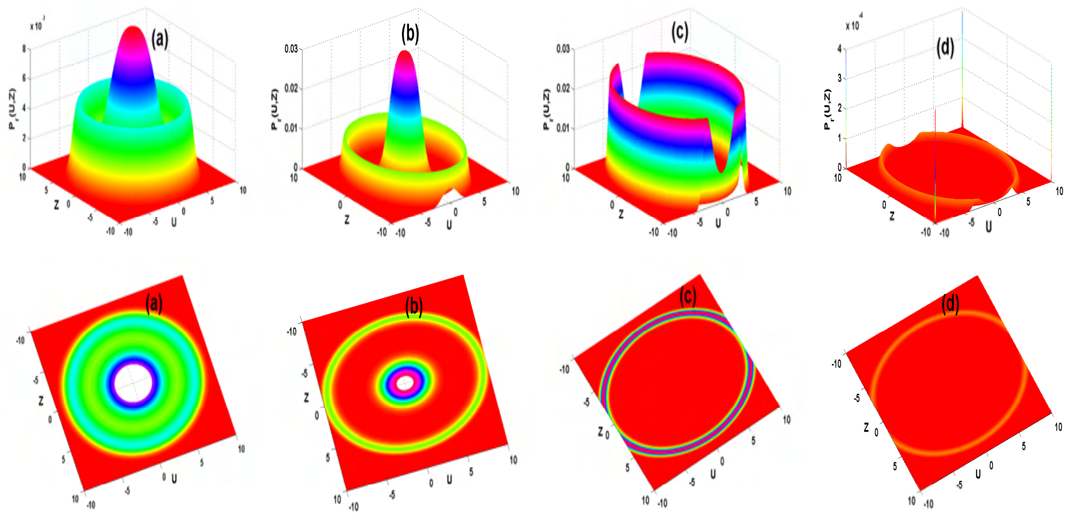

FIG. 14: *3D images of the generating joint transition spectral probability density function* $P_r(U, Z)$ *of displacement* U *and velocity* Z *for four distinct restitution coefficient numbers:* $(a) \mapsto r = 0.999$, $(b) \mapsto r = 0.96$, $(c) \mapsto r = 0.92$, $(d) \mapsto r = 0.86$. *The others selected parameters are:* $\mu_0 = 0.05$, $(\alpha_0, \beta_0, \gamma_0, \delta_0) = (0.144, 0.005, 5.82 \times 10^{-5}, 2.13 \times 10^{-7})$, $D = 0.25$, $\tau = 0.5$.

and a qualitatively different shape in the stationary PDF compared to variations in the restitution coefficient. In the trirhythmic model featuring a fractional derivative, the results illustrate that the assumed Fokker-Planck equation reveals an effective potential topology that separates the several attractors with variable frequencies. This describes the considerable stability disparities between coexisting attractors causing trirhythmicity. Besides, the restitution coefficient might randomly prevent the bifurcation, resulting in trirhythmicity.

B. Implications of restitution coefficient and fractional-order on Hopf bifurcation

In the fractional vibro-impact system, a Hopf bifurcation is a type of local bifurcation where a stable fixed point of the system transitions into an unstable state, giving rise to a small-amplitude limit cycle originating from the fixed point. In the fractional new modified vibro-impact system, a supercritical Hopf bifurcation is defined by a stable limit cycle emerging from zero amplitude and increasing in magnitude. This part investigates the Hopf bifurcation in a fractional-order trirhythmic vibro-impact device using numerical predictor-corrector estimations. The critical order of fractional-order derivatives occurs when the model suffers a Hopf bifurcation and the limit

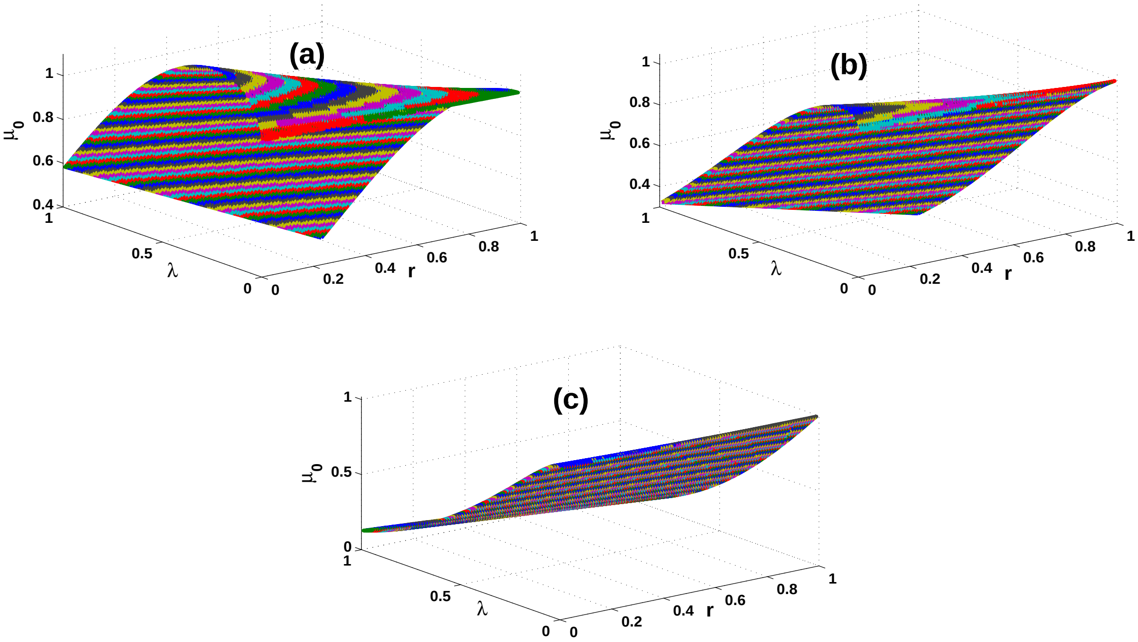

FIG. 15: numerical examination of Nonlinear parameter versus fractional-order λ and restriction coefficient r showing the non-oscillation domain for different value of natural frequency ω_0: $(a) \mapsto \omega_0 = 0.9$, $(b) \mapsto \omega_0 = 0.5$, $(c) \mapsto \omega_0 = 0.3$. The selected parameters are: $(\alpha_0, \beta_0, \gamma_0, \delta_0) = (0.144, 0.005, 5.862.10^{-5}, 2.13.10^{-7})$ $D = 0.0$.

cycle has zero amplitude. In Figure.15, we use the predictor-corrector approach with zero correlated noise intensity to represent the demarcation line between oscillation and no oscillation for the fractional new adjusted trirhythmic vibo-impact self-sustaining system. With decreasing ω_0, the separation between oscillation and no oscillation changes significantly. Consequently, we delineate the demarcation between oscillatory and non-oscillatory zones for the fractional-order extended vibro-impact van der Pol oscillator (1).

A Hopf bifurcation happens as λ and r change. In Figure.16, we depicted the nonlinear parameter as a function of λ with a fixed ω_0, showing the surface (μ_0, r) where there is no oscillation. The blue area on these figures represents the critical surface, showing the parameter zone for the non-oscillatory regime, while the white area indicates oscillation. This emphasizes the impact of λ and r on these domains, excluding any influence from the selected control parameters $(\alpha_0, \beta_0, \gamma_0, \delta_0)$.

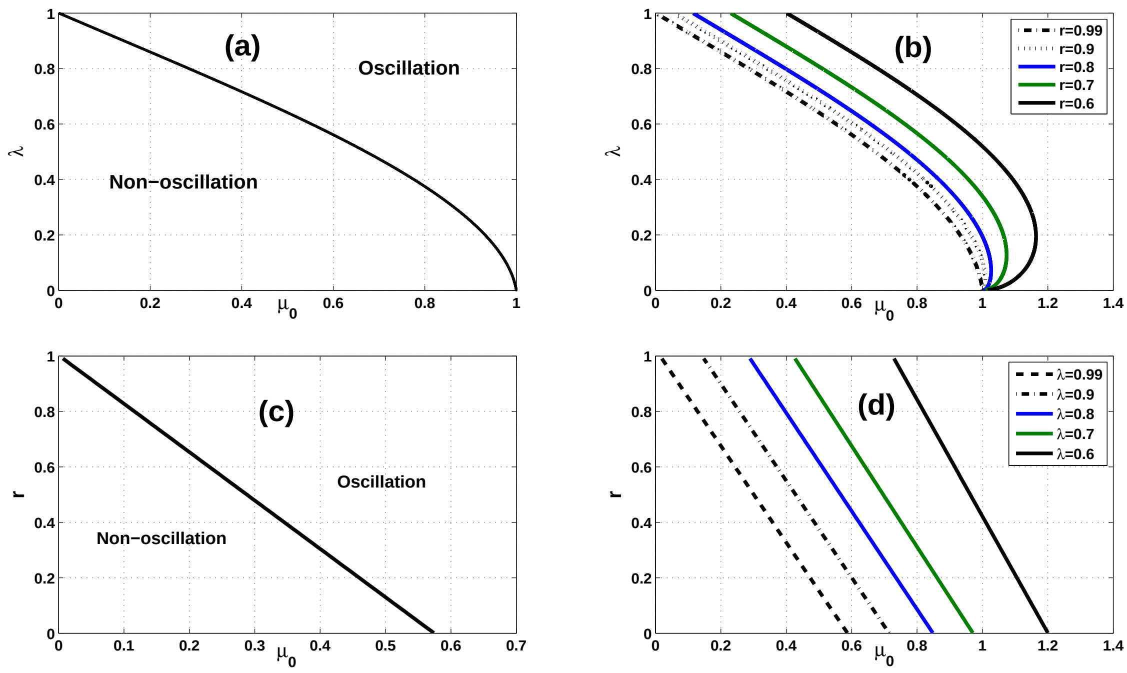

FIG. 16: (a),(c): Oscillation and non-oscillation areas for system (1) in $(\mu_0, \lambda) - plane$ (when $r = 0.99$), and (μ_0, r) (when $\lambda = 0.999$) respectively. (b), (d): Effect of restitution parameter and fractional-order respectively on the oscillation and non-oscillation regions in (μ_0, λ)-plane and (μ_0, r)-plane respectively. The selected parameters are: $(\alpha_0, \beta_0, \gamma_0, \delta_0) = (0.144, 0.005, 5.862.10^{-5}, 2.13.10^{-7})$ $D = 0.0$.

1. Investigation regarding the Lyapunov exponent using the fractional trirhythmic vibro-impact model.

The study now examines the stability of the vibro-impact model with fractional derivative and trimodal behavior in the presence of additive correlated noise, which is connected to the sudden sign change of the Lyapunov exponent. Lyapunov exponents describe how a model behaves close to its attractor. An approximation must be available for certain quantities in the trirhythmic vibro-impact model under fractional derivative. Lyapunov exponents characterize the mean exponential expansion or convergence along paths with slightly different starting circumstances and can be used to noisy systems. Our study emphasizes upon the way the correlated noise intensity D, fractional order, and restitution coefficient affect the vibro-impact system with fractional derivative acceleration, in order to discover sudden swings in the maximum Lyapunov exponent. Indeed, in Figs.17 and 18, we present the variation of the largest Lyapunov exponent versus noise intensity when $(\alpha_0, \beta_0, \gamma_0, \delta_0) = (0.144, 0.005, 5.862.10^{-5}, 2.13.10^{-7})$ for various values of μ_0 (Fig.17(a)), τ (Fig.17(b)), λ (Fig.18(a)) and r (Fig.18(b)) of the fractional vibro-impact model. These statistics

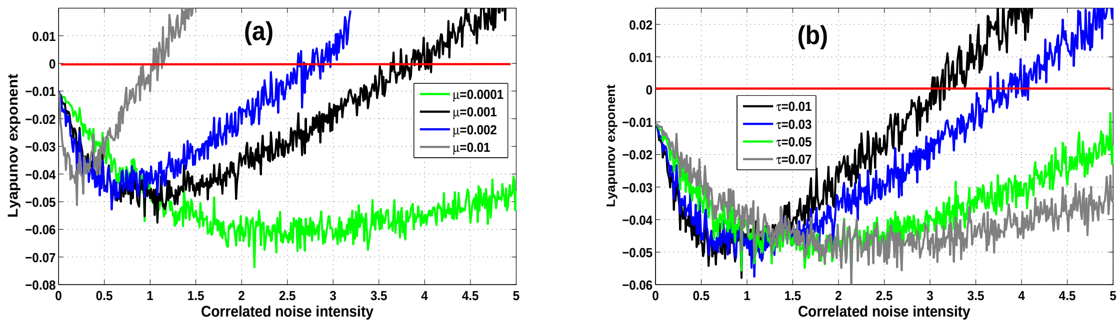

FIG. 17: (a): Variation of the average Lyapunov exponent versus correlated noise intensity for four values of nonlinear parameter μ_0 when $\tau = 0.06$. (b):Variation of the average Lyapunov exponent versus correlated noise intensity for four values of correlation time τ when $\mu_0 = 0.001$. the set parameters are: $(\alpha, \beta, \gamma, \delta) = (0.144, 0.005, 5.862.10^{-5}, 2.13.10^{-7})$ $\lambda = 0.995$, $r = 0.998$, $\omega_0 = 0.9$.

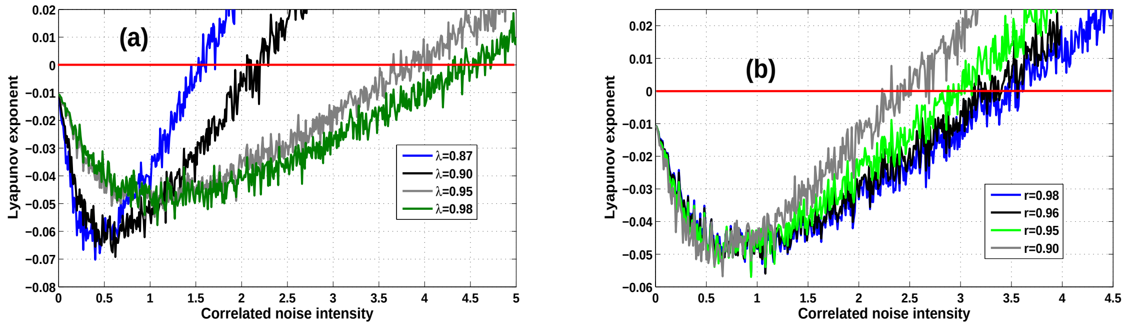

FIG. 18: (a): Evaluation of the average Lyapunov exponent versus D for four values of fractional-order λ when $r = 0.998$. (b): Evaluation of the average Lyapunov exponent versus correlated noise intensity for four values of restitution coefficient r when $\lambda = 0.998$. the selected parameters are: $(\alpha_0, \beta_0, \gamma_0, \delta_)) = (0.144, 0.005, 5.862.10^{-5}, 2.13.10^{-7})$ $\mu_0 = 0.001$, $\tau = 0.025$.

indicate that once the correlated noise reaches a certain value, the system transitions into chaos. The extremely important value of D_c represents the highest intensity of correlated noise that allows for a stable cycle. Past this threshold, disorder disrupts the system, leading to unpredictability not just in the amplitude but also the period of the oscillation. When the noise level reaches the critical value D_c, the maximum Lyapunov exponent turns positive and the system transitions to chaos. Fig.19 illustrates the variation in critical value of correlated noise intensity with respect to μ_0 (Fig.19(a)), τ (Fig.19(b)), λ (Fig.19(c)), and r (Fig.19(d)). It is observed that the critical value decreases with higher nonlinear parameter and increases with rising correlation time, fractional-

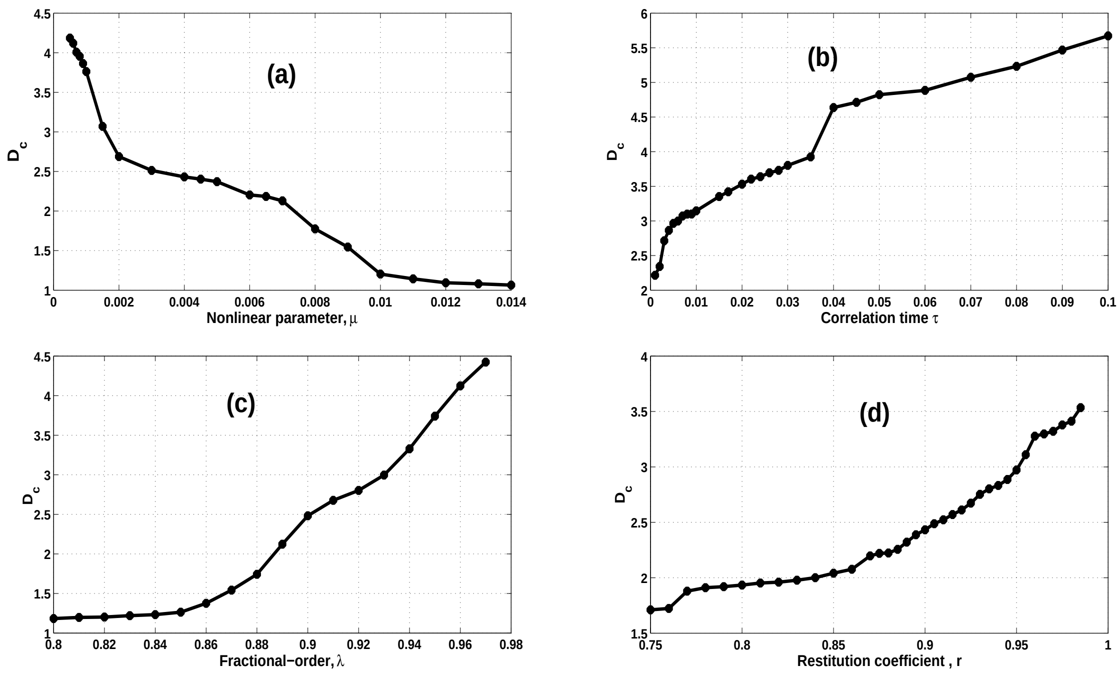

FIG. 19: (a): Critical correlated noise boundary versus nonlinear parameter μ_0 when $\lambda = 0.998$, $r = 9.998$, $\tau = 0.5$. (b):Critical correlated noise boundary versus correlation time τ when $\lambda = 0.998$, $r = 9.998$, $\mu_0 = 0.01$. (c): Critical correlated noise boundary versus fractional-order λ when $\mu_0 = 0.01$, $r = 9.998$, $\tau = 0.5$. (d):Critical correlated noise boundary versus restitution coefficient r when $\lambda = 0.998$, $\mu_0 = 0.01$, $\tau = 0.5$. The selected parameters are: $(\alpha_0, \beta_0, \gamma_0, \delta_0) = (0.144, 0.005, 5.862.10^{-5}, 2.13.10^{-7})$

order, and restitution coefficient.

As correlated noise intensity increases, it is evident that the model experiences a progressive increases in disorder, as correlated noise is believed to be detrimental to organized physical systems.

V. CONCLUSION

This article explores the behavior of a novel adapted vibro-impact self-sustained extended biological model with fractional derivative, exposed to correlated noise and with multiple limit cycles in the determinism scenario. Initially, we acquired rough estimates using a non-smooth transformation and stochastic averaging technique. Numerical results confirm the efficacy of the proposed method.We thoroughly examined bifurcation graphs in the parameters plane, and it is evident that the respective fractional-order and the restitution coefficient can be regarded as bifurcation parameters. Nonlinear terms, noise intensity, correlation time, restitution coefficient, and fractional order all have a major effect on trirhythmic features. Employing the $predictor - corrector$ algorithm and Monte Carlo calculations in numerical simulations of the distinctive system, it is discovered that the fractional-order, correlated noise parameters, and restitution parameter cause a stochastic P-bifurcation in the fractional self-sustained vibro-impact model. The development of the bifurcation point in the joint PDF follows a more developed trend than the stationary PDF for the amplitude regulated by the restitution coefficient. The PDFs can have one, two, or three peaks, demonstrating stochastic bifurcation. By exploring the joint probability density function for the aforementioned bifurcation parameters, we realized that the restitution coefficient has an enormous effect on the bifurcation dynamics of the fractional-order vibro-impact system, whereas adjustments in the restitution parameter affect other parameters. On the other hand, the bifurcations induced by fractional-order in the vibro-impact system driven by the trirhythmic behavior are more varied. Our discovery on the modified van der Pol oscillator could be useful for engineers in controlling physical motion. As a result, we anticipate that the findings of this investigation will be useful in oscillator control along with design. It has been established that there exists a critical amount of correlated noise D_c, contributing to the system to shift into chaos, which is greatly influenced by system characteristics such as μ_0, τ, r, and λ.

Data Availability Statement

The simulation data for the current study are not publicly accessible, however they can be obtained through the corresponding author, RMY, upon an adequate request.

Declarations, Conflict of interest

The authors state that they have no conflict of interest in the publishing of this work.

Acknowledgement

R.Y.M. undertook this work with the support of the German Academic Exchange Service(DAAD), Germany. He acknowledges the support of the Potsdam Institute for Climate Impact Research (PIK), Potsdam,Germany.

[1] Xu J and Chung K. W, Effects of time delayed position feedback on a van der Pol Duffing oscillator, Physica D, 180 (2003) 17-39.

[2] Rong H, Wang X, Xu W, Fang T, Resonant response of a non-linear vibro-impact system to combined deterministic harmonic and random excitations, International Journal of Non-Linear Mechanics 45 (2010) 474-481.

[3] Yang Y, Xu W and Yang G, Bifurcation analysis of a noisy vibro-impact oscillator with two kinds of fractional derivative elements, CHAOS 28, 043106 (2018)

[4] Sun H. G, Chen W, Wei H, and Chen Y. Q, A comparative study of constant-order and variable-order fractional models in characterizing memory property of systems, European Physical Journal Special Topics 193, 185 (2011)

[5] Spanos P. D and Zeldin B, Random vibration of system with frequency dependent parameters or fractional derivatives, Journal of Engineering Mechanics **123**, 290 (1997).

[6] Wang J, Yang Z, Sun W, Zhang J, Response analysis of the vibro-impact system under fractional-order joint random Excitation, Journal of law frequency noise, vibration and active control, 43(3) 10651081 (2024)

[7] Kumar P, Narayanan S, Gupta S, Bifurcation Analysis of a Stochastically Excited Vibro-impact Duffing-Van der Pol Oscillator with Bilateral Rigid Barriers, International Journal of Mechanical Sciences (2016)

[8] Ren Z, Chen J, Wang T, Zhang Z, Zhao P, Liu X, Xie J, Main sub-harmonic joint resonance of fractional quintic van der Pol-Duffing oscillator, Nonlinear Dynamics, 112, 17863-17880 (2024)

[9] Mbakob Y. R, Afungchui D , Coherence and stochastic resonance in the fractional-birhythmic self-sustained system subjected to fractional time-delay feedback and Lévy noise, Chaos, Solitons and Fractals 165 (2022) 112753

[10] Diethelm K, Ford N.J, Freed A.D, A predictor-corrector approach for the numerical solution of fractional differential equations, Nonlinear Dynamics (2002);29:3-22

[11] Srivastava H. M, Dubey V. P, Kumar R, Singh J, Kumar D, Baleanu D, An efficient computational approach for a fractional-order biological population model with carrying capacity, Chaos, Solitons and Fractals 138 (2020) 109880

[12] Mbakob Y. R, Guimfack B. A, Tabi C. B, Mohamadou A, Kofané T. C, Dynamics of a new modified

self-sustained biological trirythmic system with fractional time-delay feedback under correlated noise, Nonlinear Dynamics (2022)

[13] Kumar D, Nama H, Baleanu D, Numerical and computational analysis of fractional order mathematical models for chemical kinetics and carbon dioxide absorbed into phenyl glycidyl ether, Results in Physics 53 (2023) 107003

[14] Lin Z, Wang H, Modeling and Application of Fractional-Order Economic Growth Model with Time Delay, Fractal and Fractional (2021), 5, 74. https://doi.org/10.3390/ fractalfract5030074

[15] Din A, Khan F. M, Khan Z. U, Yusuf A, Munir T, The mathematical study of climate change model under nonlocal fractional derivative, Partial Differential Equations in Applied Mathematics 5 (2022) 100204

[16] Mbakob Y. R, Yamapi R, Filatrella G, Time delay feedbacks enhanced bifurcation in the birhythmic fractionalself-sustained system subjected to correlated noise, International Journal of Non-Linear Mechanics 154 (2023) 104429

[17] Anjum N and Ain Q. T. Application of He 's fractional derivative and fractional complex transform for time fractional Camassa-Holm equation. Thermal Sciences (2020); 24(5): 3023-3030

[18] Ahmad H, Khan TA, Ahmad I, Ahmad I, Stanimirovic P. S, Chu Y, A new analyzing technique for nonlinear time fractional Cauchy reaction-diffusion model equations. Results in Physics (2020); 19: 103462.

[19] Feudo S. L, Job S, Cavallo M, Fraddosio A, Piccioni M. D, Tafuni A, Finite contact duration modeling of a Vibro-Impact Nonlinear Energy Sink to protect a civil engineering frame structure against seismic events, Engineering Structures 259 (2022) 114137

[20] Zhang C. L, Lai Z. H, Li M. Q, Yurchenko D, Wind energy harvesting from a conventional turbine structure with an embedded vibro-impact dielectric elastomer generator, Journal of Sound and Vibration. 487 , 115616 (2020)

[21] Xu X, Qiao Z, Lei Y, Repetitive transient extraction for machinery fault diagnosis using multiscale fractional order entropy infogram,Mechanical Systems and Signal Processing 103 (2018) 312326

[22] Feng J, Xu w and Wang R, Stochastic responses of vibro-impact duffing oscillator excited by additive Gaussian noise, Journal of Sound and Vibration 309(2008): 730738.

[23] Venkatramani J, Sarkar S, Gupta S, Intermittency in pitch-plunge aeroelastic systems explained through stochastic bifurcations. Nonlinear Dynamics (2018). 92(3), 1225-1241

[24] Nganso N. E, Mbakob Y. R, Filatrella G, Yamapi R, Multi-rhythmic oscillations and correlated noise

effects of a self-sustaining biological system, Nonlinear Dynamics (2022)

[25] Li G, Ding W, Global behavior of a vibro-impact system with asymmetric clearances, Journal of sound and vibration, 423 (2018) 180-194

[26] Nordmark A. B, Non-periodic motion caused by grazing incidence in an impact oscillator, Journal of Sound and Vibration 145(2), 279297 (1991)

[27] Xie J, and Ding W, $Hopf-Hopf$ bifurcation and invariant torus T2 of a vibro-impact system, Physics Letters A 349(5):324330 (2006)

[28] Cone K. M and Zadoks R. I, A numerical study of an impact oscillator with the addition of dry friction, Journal of sound and vibration, 188:5 (1995), 659683.

[29] Dimentberg M. F and Iourtchenko D. V, Random vibrations with impacts: a review, Nonlinear Dynamics. 36:2-4 (2004), 229254. MR 2005c:74038

[30] Stefani G, Angelis M. D, Andreaus U, Influence of the gap size on the response of a single-degree-of-freedom vibro-impact system with two-sided constraints: Experimental tests and numerical modeling, International Journal of Mechanical Sciences 206 (2021) 106617

[31] Yang G, Xu W, Feng J, et al. Response analysis of Rayleigh-Van der Pol vibroimpact system with inelastic impact under two parametric white-noise excitations. Nonlinear Dynamics (2015); 82(4): 1797-1810.

[32] Zhao X, Xu W, Yang Y, et al. Stochastic responses of a viscoelastic-impact system under additive and multiplicative random excitations. Communications in Nonlinear Science and Numerical Simulation (2016); 35: 166- 176.

[33] Paola M. D, Failla G, Pirrotta A, Stationary and non-stationary stochastic response of linear fractional viscoelastic systems, Probabilistic Engineering Mechanics 28, 8590 (2012)

[34] Mickens R. E , Oscillation in Planar Dynamic Systems, World Scientific, Singapore, (1996).

[35] Luo A. C. J and Chen L, Periodic motions and grazing in a harmonically forced, piecewise, linear oscillator with impacts, Chaos, Solitons and Fractals. 24:2 (2005), 567578.

[36] Padmanabhan C and Singh R, Analysis of periodically excited non-linear systems by a parametric continuation technique, Journal of sound and vibration 184:1 (1995), 3558.

[37] Xie X, Li J, Liu D, Guo R, Transient response of nonlinear vibro-impact system under Gaussian white noise excitation through complex fractional moments, Acta Mechanica 228 (2017), 11531163

[38] Eichhorn R, Linz S. J, $H\ddot{a}nggi$ P, Transformation invariance of Lyapunov exponents, Chaos, Solitons and Fractals 12 (2001) $1377-1383$

[39] Xiao Y, Xu W and Wang L, Stochastic responses of Van der Pol vibro-impact system with fractional derivative damping excited by Gaussian white noise, CHAOS 26, 033110 (2016)

[40] Yurchenko D, Burlon A, Paola M. D, Failla G, Pirrotta A, Stochastic response of a fractional vibroimpact system, Procedia Engineering 199 (2017) 10861091

[41] Yang Y, Xu W, and Yang G, Bifurcation analysis of a noisy vibro-impact oscillator with two kinds of fractional derivative elements, Chaos 28, 043106 (2018)

[42] Zhuravlev V, A method for a nalyzing vibration-impact systems by means of special functions, Mechanics of Solids 11(2), 2327 (1976)

[43] Li C, Xu W, Feng J, Wang L, Response probability density functions of Duffing-Van der Pol vibro-impact system under correlated Gaussian white noise excitations, Physica A 392 (6), 12691279 (2013)

[44] Liu L, Xu W, Yue X, Han Q, Stochastic response of Duffing-Van der Pol vibro-impact system with viscoelastic term under wide-band excitation, Chaos, Solitons and Fractals 104 (2017) 748757

[45] Kumar A, Alam K, Rahman M, Emadifar H, Arora G, Hamoud A, Fractional Stochastic Van der Pol Oscillator with Piecewise Derivatives, Journal of Mathematics (2024), https://doi.org/10.1155/2024/2436203

[46] Zhang J, Wang F, Wang H, Fractional stochastic vibration system under recycling noise, Frontiers in Physics (2023), 11:1238901.

[47] Ngo M. A, Kammogne S. T. A, Kengne R, Fotsin H. B., Essimbi Z. B, Effect of Fractional-Order on the Dynamic of two Mutually Coupled van der Pol Oscillators: Hubs, Multistability and its Control , Discontinuity, Nonlinearity, and Complexity 9(1) (2020) 83–98, DOI:10.5890/DNC.2020.03.007

[48] Mirzazadeh M, Ekici M, Eslami M, Krishnan E. V, Kumar S, Biswas A, Solitons and other solutions to Wu-Zhang system, Nonlinear Analysis: Modelling and Control (2017), Vol. 22, No. 4, 441-458

[49] Xu L, Yin X, Cao N, Bai S, Multi-soliton solutions of a variable coefficient $Schrödinger$ equation derived from vorticity equation. Nonlinear Dynamics (2024) 112, 2197-2208.

[50] Marwan N, Romano M. C, Thiel M, Kurths J, Recurrence Plots for the Analysis of Complex Systems, Physics Reports 438, (2007).